AEDC-TR-78-39

IN SITU OPTICAL TECHNIQUES FOR JET ENGINE EXHAUST HYDROCARBON DETECTION

C. J. Fisher
ARO, Inc., a Sverdrup Corporation Company

ENGINE TEST FACILITY
ARNOLD ENGINEERING DEVELOPMENT CENTER
AIR FORCE SYSTEMS COMMAND
ARNOLD AIR FORCE STATION, TENNESSEE 37389

November 1978

Final Report for Period September 1976 — October 1977

Approved for public release; distribution unlimited

Prepared for

NAVAL AIR PROPULSION CENTER
TRENTON, NEW JERSEY 08628

This report has been reviewed by the Information Office (OI) and is releasable to the National Technical Information Service (NTIS). At NTIS, it will be available to the general public, including foreign nations.

APPROVAL STATEMENT

This report has been reviewed and approved.

EULES L. HIVELY
Project Manager, Research Division
Directorate of Test Engineering

Approved for publication:

FOR THE COMMANDER

ROBERT W. CROSSLEY, Lt Colonel, USAF
Acting Director of Test Engineering
Deputy for Operations

UNCLASSIFIED

REPORT DOCUMENTATION PAGE		READ INSTRUCTIONS BEFORE COMPLETING FORM
1 REPORT NUMBER AEDC-TR-78-39	2 GOVT ACCESSION NO.	3 RECIPIENT'S CATALOG NUMBER
4 TITLE (and Subtitle) IN SITU OPTICAL TECHNIQUES FOR JET ENGINE EXHAUST HYDROCARBON DETECTION		5 TYPE OF REPORT & PERIOD COVERED Final Report - September 1976 - October 1977
		6 PERFORMING ORG REPORT NUMBER
7 AUTHOR(s) C. J. Fisher, ARO, Inc., a Sverdrup Corporation Company		8 CONTRACT OR GRANT NUMBER(s)
9 PERFORMING ORGANIZATION NAME AND ADDRESS Arnold Engineering Development Center Air Force Systems Command Arnold Air Force Station, TN 37389		10. PROGRAM ELEMENT PROJECT TASK AREA & WORK UNIT NUMBERS 921B05
11. CONTROLLING OFFICE NAME AND ADDRESS Naval Air Propulsion Center P. O. Box 7176 Trenton, NJ 08628		12. REPORT DATE November 1978
		13 NUMBER OF PAGES 65
14 MONITORING AGENCY NAME & ADDRESS(if different from Controlling Office)		15. SECURITY CLASS. (of this report) UNCLASSIFIED
		15a DECLASSIFICATION/DOWNGRADING SCHEDULE N/A

16 DISTRIBUTION STATEMENT (of this Report)

Approved for public release; distribution unlimited.

17 DISTRIBUTION STATEMENT (of the abstract entered in Block 20, if different from Report)

18 SUPPLEMENTARY NOTES

Available in DDC.

19 KEY WORDS (Continue on reverse side if necessary and identify by block number)

gas analysis
high resolution spectroscopy
interferometric spectroscopy
hydrocarbons
infrared spectroscopy
emission
exhaust gases

20 ABSTRACT (Continue on reverse side if necessary and identify by block number)

An investigation was conducted to determine the feasibility of developing an in situ optical technique suitable for jet engine exhaust diagnostics of gaseous hydrocarbon concentrations. The initial approach involved the evaluation of several possible techniques. Two absorption spectroscopy techniques were investigated: (1) high-resolution interferometric spectroscopy in the 2,800- to 3,250-cm^{-1} region of the IR and (2) the absorption of

DD $_{1\ JAN\ 73}^{FORM}$ 1473   EDITION OF 1 NOV 65 IS OBSOLETE

UNCLASSIFIED

20. ABSTRACT (Continued)

the radiation of a modified He-Ne laser emitting in the IR. A candidate for use as a radiation source in a correlation spectrometer, a microwave-excited methane infrared source, was also evaluated. Another spectroscopic technique, the detection of CH visible emission, was also investigated. As a means of investigating the possible effects of mechanical probing on the chemical identity and hence the spectroscopic properties of the hydrocarbon constituents of exhaust gases, a simulation of the effects of probing on methane containing exhaust constituents was performed. A preliminary investigation of the gaseous hydrocarbon content of a combustor using in situ optical probing and online conventional gas analyzers as well as optical probing and laboratory gas analysis of samples drawn with an orifice-type emissions probe is also reported. It was concluded that the best approach to in situ gaseous hydrocarbon detection may be a multiple-pass, tuneable diode laser system.

AFSC
Arnold AFS Tenn

PREFACE

CONTENTS

ILLUSTRATIONS

TABLES

APPENDIX

1.0 INTRODUCTION

Composition determination of flowing hot gas mixtures has traditionally been accomplished with probe extraction techniques and conventional commercial gas analyzers. With these techniques the probe orifice is positioned perpendicular to the flow, and the gas extracted is brought to a standard temperature and pressure before analysis. In recent years the ability of probe sampling to preserve the chemical identity of the sample gas has been seriously questioned (Refs. 1 through 5). Reactions in the altered flow field approaching the probe and the continued reaction of the constituents in the probe, either in the gas phase or on a surface, are a real possibility. In addition to this problem, in many applications, physical limitations render the use of probe technology impractical.

For these reasons there has been a great deal of interest in noninterference, *in situ* optical techniques of combustion gas diagnostics. Techniques which have been developed or proposed include molecular spectral absorption [infrared (IR) and ultraviolet-visible (UV-VIS)] from line (laser or discharge) or continuous sources, thermal emission, laser-induced fluorescence and Raman spectroscopy, and coherent anti-stokes Raman spectroscopy (CARS).

The ultimate objective of the program reported herein is to develop a practical *in situ* optical hydrocarbon diagnostic technique. An *in situ* technique capable of being calibrated independently of probe technology could provide a means of defining the limits of validity of current probe techniques as well as replace some of these techniques in field applications. This report addresses the problems of the development and implementation of a gaseous hydrocarbon *in situ* optical technique suitable for jet engine exhaust diagnostics and reports on experimental and theoretical progress toward this goal.

Strictly speaking, the term "hydrocarbon" denotes compounds consisting of only carbon and hydrogen. Through common usage, however, the term has come to denote not only the true hydrocarbons but also the partially oxidized species such as alcohols, aldehydes, ketones, esters, and organic acids, as well as compounds containing nitrogen, sulfur, and other elements in addition to carbon and hydrogen. In this report the more general definition will be used.

The initial approach of this study involved the evaluation of several possible techniques. Two absorption spectroscopy techniques were investigated: (1) high-resolution interferometric spectroscopy in the 2,800- to 3,250-cm^{-1} region of the IR and (2) the absorption of the radiation of a modified helium-neon (He-Ne) laser emitting in the IR. A candidate for use as a radiation source in a correlation spectrometer, a microwave-excited methane infrared source, was also evaluated. Another spectroscopic technique, the

detection of CH visible emission was also investigated. As a means of investigating the possible effects of mechanical probing on the chemical identity and hence the spectroscopic properties of the hydrocarbon constituents of exhaust gases, a simulation of the effects of probing on methane containing exhaust constituents was performed. A preliminary investigation of the gaseous hydrocarbon content of a combustor using *in situ* optical probing and online conventional gas analyzers as well as optical probing and laboratory gas analysis of samples drawn with an orifice-type emissions probe is also reported.

2.0 BACKGROUND

The standard modern analyzer for "total hydrocarbon" (THC) concentrations is the flame ionization detector (FID). In this device a drawn sample is mixed at a standard rate with a hydrogen-air flame. When the flame is exposed to an electric field, the resultant current is very nearly proportional to the sum of the hydrocarbon concentrations as weighted by the number of carbon atoms per species (ppmc). Thus this measurement is related to the volume concentration (ppmv) by the relationship

$$ppmc = \sum_{\substack{i = all \\ HC \; species}} c_i \; ppm \; \nu_i$$

$$(1)$$

where c_i is the number of carbon atoms of species "i". The uniformity of response of the FID with respect to chemical species is excellent (Ref. 6). A properly adjusted instrument will give on the order of ±5-percent uniformity of response for paraffins, olefins, acetylenes, and aromatics with little interference effects. The instrument is calibrated against a known concentration of a reference hydrocarbon, usually methane, and the results of the measurements are called methane equivalents.

An earlier study of the hydrocarbon content of the exhaust of a T-56 combustor by Conkle et al. (Ref. 7) used probe-extracted samples, cryogenic trapping, gas chromatography, and mass spectroscopy for identification. Although this study was not quantitative and the collection procedures omitted methane (CH_4) and possibly other light hydrocarbons, it yielded the first detailed hydrocarbon composition data for combustor exhausts. It also revealed some of the problems that would need to be overcome in developing an *in situ* technique. The study identified 273 distinct compounds, none of which at any power setting was found in concentrations in excess of 14 ppm. The vast majority had concentrations significantly less than 1 ppm.

8

The possibility of the use of laser Raman and/or laser-induced fluorescence as a diagnostic technique is being intensively investigated by D. A. Leonard, whose experimental design represents the limit of current technology. In his latest report (Ref. 8) Leonard indicates that the hydrocarbon Raman signals are not observable in the exhaust of a T-53 engine, but that the intensity of the continuum (to 5,500Å) fluorescence excited by a 3,371Å nitrogen laser is roughly proportional to the THC concentration as determined with an FID analyzer. Since the source of this fluorescence is not identifiable, it appears that this approach will not lead to a technique which will be calibratable independent of probe extraction technology.

Roquemore and Hodgson (Ref. 9) found that when a T-56 exhaust gas was bubbled through cooled solvent it fluoresced in the same spectral region as that noted by Leonard. They ascribe this fluorescence to multiple-ring aromatics, relatively minor constituents of the exhaust gas.

Lazalier and Gearhart (Ref. 10) studied hydrocarbon emissions from a J85-GE-5 engine using probe extraction techniques and FID detection. They found THC concentrations on the order of 700 ppmc at idle, 50 to 100 ppmc at cruise and military power, and as high as 6,400 ppmc at a power setting of midafterburning. The THC, however, declined at 4.9 m downstream of the nozzle exit for all power settings.

Davidson and Domal (Ref. 11) made emission measurements at the nozzle exit of a J93 turbojet engine. At simulated conditions of Mach number 2.0 and 19.8 km altitude at military power they found 10 to 12 ppmc THC. At the same conditions at maximum afterburning they found from 30 to 4,700 ppmc THC. They also report some gas chromatographic analyses of extracted samples yielding molecular weight distributions and methane analyses.

In summary, to date there has been no successful *in situ* measurement of hydrocarbons in combustor or jet exhausts, but several studies have provided significant useful data which might aid in the development of a workable technique.

3.0 INFRARED INTERFEROMETRY SPECTRA STUDIES

A considerable effort was directed toward the investigation of the absorption of gaseous hydrocarbons from a continuum in the 2,800- to 3,250-cm^{-1} region of the IR. This region was selected because it contains carbon-hydrogen stretching bands for all hydrocarbons. It also is relatively free of interfering absorptions of species normally found in plumes (CO_2, H_2, CO, NO, and NO_2) except for some lines of water vapor.

The study included the measurement of the temperature and concentration dependence of line absorption of gaseous CH_4 diluted in nitrogen (N_2), the temperature dependence of n-heptane vapor in N_2 absorption, and attempts at recording spectra of toluene and propylene vapor diluted with N_2 in a quartz absorption cell. In addition, the CH_4 absorptions were computer simulated, and detectability limits as a function of temperature and pathlength were calculated.

3.1 EXPERIMENTAL APPARATUS

High-resolution measurements of the hydrocarbon spectra were made with an AEDC EOCOM high-resolution Fourier transform spectrometer model 7101, which is a Michelson interferometer with appropriate position-monitoring and data-recording instrumentation. It is equipped with a cooled indium-antimonide (InSb) detector and a calcium fluoride beam splitter. The maximum resolution is 0.06 cm^{-1}. The spectral range of this instrument was restricted from 2,800 to 3,250 cm^{-1} by an interference filter at the detector and two electronic bandpass filters.

The interferograms contained 64.000 points and were recorded on magnetic tape and later transformed on the AEDC IBM 370 computer system by an EOCOM-supplied program and a program developed at AEDC.

The samples were contained in a 50.7- by 7.6-cm-diam quartz absorption tube with fused Infrasil® No. 2 windows. This cell was heated in a tube furnace. A Globar® was used as the continuum source. Its image was focused by a 15-cm Cassegrainian telescope at the center of the cell and was transmitted to the interferometer as a 5-cm-diam collimated beam by a 20.3-cm Cassegrainian telescope. Background emission spectra at elevated temperatures were recorded in the same configuration, with the Globar blocked. A photograph of the experimental instrumentation is displayed in Fig. 1.

3.2 METHANE ABSORPTION RESULTS AND ANALYSIS

In this section the absorption spectra of gaseous CH_4 diluted with N_2 at various temperatures and concentrations, the theoretical development required for the calculation of molecular concentrations from integrated narrow-line absorptions, and the comparison of these calculations to the CH_4 data are presented.

3.2.1 Curve of Growth Theory

A curve of growth analysis is required to calculate molecular concentration from the integrated absorbances of isolated narrow spectral lines which are broadened by both Doppler and collisional broadening. The analysis relates a quantity proportional to the

number density of the absorbing species in the ground absorbing state multiplied by the optical pathlength and the strength of the transition to the integrated area under an absorption line. The results of the calculations are usually presented as a universal plot employing reduced variables, making it possible to correlate data taken at different temperatures, pressures, and concentrations. The ordinate of the plots is

$$\frac{N_i f_i \ell \sqrt{\ell n 2}}{\pi \, \Delta \nu_D \, c}$$

where N_i is the number density (molecules/cc) of the absorbing species in the ground absorbing state "i," f_i is the f-number, a measure of the strength of the transition (dimensionless), ℓ is the pathlength (cm), $\Delta \nu_D$ is the Doppler width (cm^{-1}), and c is the speed of light (2.998 x 10^{10} cm sec^{-1}). The abscissa of the plots is $A_G \sqrt{\ell n 2}/2\pi \, \Delta \nu_D$, where $A_G/2\pi$ is the area under the absorption line (cm^{-1}). Using these reduced variables, one can characterize a curve of growth by a single parameter, "a", the broadening parameter which is defined as $\Delta \nu_c \sqrt{\ell n 2}/\Delta \nu_D$ where $\Delta \nu_c$ is the collisional line width. A concise derivation of the curve of growth formulation using the above formulism is given in Ref. 12. The Fortran computer code used for this calculation is presented in Appendix A.

The Doppler width, a function of temperature and molecular weight of the absorbing species and the energy of the transition, is given by (Ref. 12)

$$\Delta \nu_D = \frac{2 \sqrt{2R \, \ell n \, 2}}{c} \, \nu_o \sqrt{\frac{T}{M}} \tag{2}$$

where "R" is the universal gas constant (8.317 x 10^{17} ergs mole^{-1}°K^{-1}), ν_o is the absorption line center position (cm^{-1}), and M is the molecular weight (16.04 g mole^{-1} for CH_4).

The parameters of interest, $\Delta \nu_c$ of CH_4 in N_2 and the "f" numbers, as well as the energy levels for the absorbing state population calculations, are available (Refs. 13 and 14). Line strength data are available in the units of integrated intensities, S_J (cm^{-2} atm^{-1}), at 300°K (Ref. 14). For the R_6 line of CH_4 the experimental S_J value is 19.2, and for R_7 it is 14.4. To use these values in the curve of growth analysis, an f'_{300} is defined as $f_i \times p_{i300}$ where p_{i300} is the fractional population in state "i" at 300°K. The quantity f'_{300} is related to S_J by the equation

$$f'_{300} = S_J \, \frac{mc^2}{\pi \, e^2 N_s} = 4.6208 \times 10^{-8} \, S_J \tag{3}$$

11

where m is the mass of an electron (9.1095×10^{-28} g), c is the speed of light, e is the charge of an electron (4.803×10^{-10} esu), and N_s is the standard number density at 101.325 kPa and 300°K (2.445×10^{19} molec. cc^{-1}). The required quantity for the curve of growth calculation, $N_i f_i$, is given by $N_{CH_4} f'_{300} \, p_T/p_{300}$ where N_{CH_4} is the CH$_4$ number density and p_T/p_{300} is the ratio of the fractional absorbing state population at temperature T to that at 300°K. Use of statistical thermodynamics shows p_T/p_{300} to be (Ref. 13)

$$\frac{p_T}{p_{300}} = \frac{\exp\left\{\dfrac{-7.557\,[J(J+1)]}{T}\right\}\Big/T^{3/2}}{\exp\left\{\dfrac{-7.557[J(J+1)]}{300}\right\}\Big/5{,}196.2} \times \frac{Q_{v300}}{Q_{vT}} \tag{4}$$

where J is the rotational quantum number of the absorbing state and Q_{v300}/Q_{vT} is the vibrational population temperature correction factor. The term Q_{vT}, the vibrational partition function at temperature T, is given by

$$Q_{vT} = \prod_{i=1}^{4}\left[1 - \exp\left(\frac{-1.4388}{T}\nu_i\right)\right]^{-g_i} \tag{5}$$

where

$$\nu_1 = 2{,}914.2 \ \text{cm}^{-1} \qquad\qquad g_1 = 1$$

$$\nu_2 = 1{,}526 \ \ \text{cm}^{-1} \qquad\qquad g_2 = 2$$

$$\nu_3 = 3{,}020.3 \ \text{cm}^{-1} \qquad\qquad g_3 = 3$$

$$\nu_4 = 1{,}306.2 \ \text{cm}^{-1} \qquad\qquad g_4 = 3$$

The vibrational population temperature correction factor accounts for the thermal depopulation of the absorbing vibrational state with increasing temperature, while the J-dependent term of p_T/p_{300} accounts for the depopulation of the absorbing rotational state. Table 1 lists the rotational correction terms, p_T/p_{300} and Q_{v300}/Q_{vT}, for the R6 and R7 lines as a function of temperature.

The CH$_4$ spectra consist of multiplet lines. Under high resolution these lines are seen to consist of several components in a region on the order of 1 cm^{-1}. An example of a CH$_4$ multiplet line, the R$_7$ line, at high resolution (0.06 cm^{-1}) and low pressure (10.13 kPa) is shown in Fig. 2. The broader line to the right at 3,095.9 cm^{-1} is an atmospheric water vapor line.

In a study by Varanasi (Ref. 15) it was shown that the collisional broadening of CH_4 by N_2 at 295°K can be represented by a single effective $\Delta\nu_c$ value which can be used for an entire multiplet line. Corrected to 97.9 kPa, the reported full width at half height of the R_6 lines is 0.122 ± 0.007 cm⁻¹ atm⁻¹, which corresponds to a broadening parameter, a, of 10.7 ± 0.6 at 295°K. The R_7 value was not reported, but the J dependence of $\Delta\nu_c$ is very weak (Ref. 15), and the R_6 $\Delta\nu_c$ value was used for both lines.

Since the temperature and number density dependence of $\Delta\nu_c$ has not been reported, it must be calculated. This was accomplished by using a hard sphere kinetic theory of gases model calculation (Ref. 16). This model shows the temperature and number density dependence to be $\Delta\nu_c \propto N_D \sqrt{T}$ where N_D is the number density of the diluent gas or cast in terms of pressure $\Delta\nu_c \propto P_D/\sqrt{T}$ where P_D is the pressure of the diluent gas. Using the latter proportionality relationship the broadening parameters "a", for CH_4 in N_2 at a total pressure of 97.9 kPa are calculated to be 10.5 at 300°K, 5.52 at 573°K, 4.09 at 773°K, 3.16 at 1,000°K, 2.11 at 1,500°K, and 1.58 at 2,000°K.

3.2.2 Experimental Results

The absorption spectra of gaseous CH_4 diluted with N_2 to a total pressure of 97.9 kPa were recorded at 297, 373, and 773°K. Concentrations of CH_4 investigated were 99.6, 498, and 996 ppm.

Fig. 3 shows the CH_4 absorption spectra of the ν_3 band from 2,800 to 3,250 cm⁻¹ at 297°K and at a concentration of 996 ppm. The dense central section at 3,017 cm⁻¹ is the Q branch. The regularly spaced lines at higher energies are members of the R branch, and the regularly spaced lines at lower energies belong to the P branch. There are also numerous extraneous lines due to water vapor absorption in the optical path, but not in the cell. These lines can be seen in the evacuated cell spectra in Fig. 4.

Two lines, the R_6 and R_7 lines, were investigated for use in a quantitative curve of growth analysis. Examples of a broadened R_6 and R_7 line are displayed in Figs. 5 and 6. Note the increase in width of the N_2-broadened R_7 line as compared to the low-pressure spectrum of Fig. 2.

The integrated absorptions, $A_G/2\pi$, required to obtain the CH_4 number densities from the curve of growth analysis were obtained by integrating with a planimeter the area under the absorption lines. Some of the lines integrated are shown in Figs. 5 through 10. Figure 5 displays the most intense absorption example of the R_6 line (996 ppm CH_4 at 97.9 kPa total pressure at 297°K). Figure 6 displays the R_7 line under the same conditions. At higher temperatures the integrated absorptions decrease because the gas is rarefied and the

absorbing state is depopulated. Figs. 7 and 8 display the R_6 line at 573°K and 773°K respectively at a concentration of 996 ppm at 97.9 kPa. Figs. 9 and 10 display the R_7 line under the same conditions.

3.2.3 Curve of Growth Analysis Results

The CH_4 R_6 and R_7 integrated line absorption data and the curve of growth calculations are presented in Figs. 11 and 12. The solid lines are the curve of growth calculations for broadening parameters, a, of 10.5, 5.52, 4.09, and 1.58, which correspond to temperatures of 300, 573, 773, and 2,000°K, respectively, at 97.9 kPa total pressure. The symbols are the result of the experimental measurements. The agreement between the calculated and experimental integrated absorptions is excellent.

It can be seen in Figs. 11 and 12 that once the thermal depopulation of the absorbing state is accounted for, the integrated absorbance is a weak function of the broadening parameter in the small optical density regime. This regime includes the spectra expected from hydrocarbon detection in jet engine exhaust applications.

3.3 METHANE DETECTABILITY LIMITS

The results of the previous section provide a means of calculating the detectability limits of CH_4 as a function of pathlength and temperature, and hence, of estimating the THC detectability limits using the data of a previous study (Ref. 11).

Figs. 13 and 14 show the absorption of the R_6 and R_7 lines of CH_4 in N_2 at a concentration of 99.6 ppm (total pressure is 97.9 kPa) at a temperature of 773°K in a 50.7-cm pathlength cell. This absorption, approximately 6 percent in both cases, was chosen to be the standard of detectability of CH_4. At different temperatures and pathlengths, the concentration of CH_4 required to match the absorption indicated in Figs. 13 and 14 was calculated and identified as the CH_4 detectability limit. The calculated CH_4 detectability limits from 300 to 2,000°K at 1-, 10-, and 50-m pathlengths for these lines are presented in Table 2. On the assumption that CH_4 constitutes approximately 1.5 percent of the THC concentration in jet engine exhausts, as has been found to be the case by Davidson and Domal (Ref. 11), estimates of the THC detectability limits were made by simply dividing the CH_4 detectability limits by 0.015. These estimates are presented in Table 3.

3.4 OTHER HYDROCARBON SPECTRA

Absorption spectra of heptane vapor were recorded at a concentration of 516.8 ppm in N_2 (total pressure 97.9 kPa) at 297, 573, and 773°K and are shown in Figs. 15 through 17. Superimposed on the spectra are the spectra of the evacuated cell at the same temperature.

14

Note that all of the sharp line absorptions are found in both systems, indicating that these lines are caused by species outside the cell (i.e., atmospheric water vapor). The heptane absorption consists of a broad band from approximately 2,840 to 2,985 cm^{-1} with the maximum absorption at 2,934 cm^{-1}. Since no fine structure is resolvable, the identification of the ground-absorbing state or states at a particular energy is impossible, and thus the calculation of the extent of the thermal depopulation is also impossible.

The Lambert-Beer absorption law for absorptions of linewidths considerably wider than the resolving power of the observing instrument with temperature effects taken into account can be written (Ref. 17) as follows:

$$\frac{I(\nu)}{I_o(\nu)} = \exp\left(-N \alpha(T) \ell\right)$$

(6)

where N is the number density of the absorbing species, $\alpha(T)$ is the molecular absorption coefficient of the observed transition, and ℓ is the pathlength. Data such as the continuous absorption of heptane can be reduced within this formalism to yield $\alpha(T)$ as a function of temperature, which can serve as a universal calibration plot for species concentration. The heptane molecular absorption coefficient as a function of temperature is displayed in Fig. 18 and is proportional to the absorbing state population. Thus a plot of this nature reveals the thermal depopulation of the absorbing state.

For absorptions of 6 percent the heptane detectability limits at 97.9 kPa and a 1-m pathlength are calculated to be 30.8 ppmv (215.6 ppmc) at 297°K, 74.3 ppmv (520.1 ppmc) at 573°K, and 148.6 ppmv (1,040.2 ppmc) at 773°K.

The two other representative hydrocarbon vapors studied were propylene and toluene. Absorption interferograms were recorded for propylene at a concentration of 999.5 ppm in N_2 and for toluene at a concentration of 533 ppm in N_2 both at 97.9 kPa and 297, 573, and 773°K in the 50.7-cm quartz absorption cell. No absorption was detected in either of these systems. The lack of absorption at these conditions indicates detectability limits of greater than 500 ppmv (1,500 ppmc) propylene and 250 ppmv (1,750 ppmc) toluene for a 1-m pathlength at the temperatures and pressures investigated.

4.0 INFRARED LASER EXPERIMENTS

From the interferometry studies (Section 3.0) it has been shown that for high sensitivity IR absorption detection of gaseous CH_4 and other hydrocarbon vapors, long pathlength-high resolution spectroscopy is required. There are two ways to achieve high resolution: (a) a high resolution spectroscopic instrument such as an interferometer or a

15

large grating spectrometer, or (b) a narrow-line, tunable laser source. A laser source offers the added advantage of high intensity per unit wavelength and beam cross-sectional area, properties which make it suitable for multiple pass applications.

A preliminary experiment was performed employing a specially modified He-Ne laser emitting radiation at 2,947.903 cm^{-1}, an energy coincident with the CH_4 P_5 multiplet line. The CH_4 P_5 line in absorption, as recorded interferometrically, is displayed in Fig. 19. The absorption of CH_4 by a He-Ne laser has been studied previously (Refs. 18 and 19).

4.1 EXPERIMENTAL DESIGN

The experimental arrangement employed is shown schematically in Fig. 20. A specially modified He-Ne laser is the source. The modification of the laser involves replacing the cavity visible reflecting mirrors with IR reflecting mirrors. The output of the modified laser is 3 mw at 3.39μ. The beam is chopped at 300 Hz and split into a primary beam and a reference beam by a quartz beamsplitter. The reference beam provides the means of continuously monitoring the laser output power. The reference beam is detected by a filter radiometer. The primary beam is directed into a White multiple-pass system and into a detector unit. The detector unit consists of an InSb detector equipped with a high-pressure nitrogen cryostat, an interference filter, and a 50-mm focal length silicon focusing lens. The signal from the detector is amplified and fed into a lock-in amplifier which controls a dual pen strip chart recorder. A conventional visible He-Ne laser is used for alignment purposes.

The gas to be analyzed was contained in an 86-cm-long, 10-cm-wide quartz absorption tube equipped with thermostated heaters, thermocouples, and a pressure transducer.

4.2 RESULTS AND DISCUSSION

With the absorption cell in place. the multiple-pass system was successfully operated in 4-, 8-, and 12-pass configurations. Reflection, absorption, and dispersion losses at the cell windows limit the number of passes possible through a cell with a given laser power and White system geometry. With no cell. 36-pass operation was achieved. The number of passes possible with a White optical system depends on the source power, reflection losses of the mirrors, losses incurred passing through the cell or absorbing medium, and geometrical optical factors such as the size of the mirrors and the focused image size.

Preliminary experiments indicate that the responses of the two laser power detectors, the transmission detector and the reference detector, did not vary together as expected. An example of this behavior is displayed in Fig. 21.

16

The two detector systems were checked for stability against a blackbody source and were found to be stable. Two other possible sources of this discrepancy are vibration of optical components or spatial fluctuations of the laser. The experiment was repeated in a simpler configuration without the multiple-pass system, and the results were similar, thus indicating that vibration of the optical components was not a factor. The other possibility, the spatial fluctuations of the laser beam, must be investigated. A possible approach to the problem might be the use of optical apertures to define and limit the laser beam. In its present form the absorption of fixed frequency IR laser radiation is not a workable hydrocarbon diagnostic technique.

5.0 MICROWAVE DISCHARGE EVALUATION

A possible source of radiation suitable for CH_4 absorption experiments is the microwave discharge radiation of low-pressure CH_4. An experiment was performed to evaluate the discharge radiation of low-pressure gaseous CH_4.

5.1 EXPERIMENTAL DETAILS

In this experiment, CH_4 at a pressure of 2.0 kPa was flowed through a 12-mm OD tube equipped with a lithium fluoride (LiF) window. A discharge cavity surrounded the tube and was powered by a microwave cavity power supply. The radiation was directed into an AEDC EOCOM interferometer by a 20.3-cm Cassegrainian telescope.

5.2 RESULTS AND DISCUSSION

The radiation emitted between 2,800 and 3,250 cm^{-1} was very weak and unstable. The reduced interferogram of the output from 2,800 to 3,250 cm^{-1} shows no discernable emission. Apparently the emitted radiation is almost obscured by the background noise of the interferometer.

Another problem experienced was the degradation of the window and tube by soot formed from the pyrolysis products of the CH_4. The collection of soot on the tube caused excessive heating, and the tube developed a leak.

In its present state of development the microwave discharge tube was found to be inadequate for the generation of suitable resonance radiation for CH_4 absorption studies. Better performance in the future might result from the use of a quartz tube, isolation of the window, and/or use of mixtures of CH_4 with other gases.

6.0 CH EMISSION STUDY

There are several advantages to working in the visible-ultraviolet (V-UV) region of the radiation spectrum rather than in the IR region. The advantages of working in the V-UV can be classified in the categories of detectors, optical materials, and thermal interferences.

The detectors of choice for the V-UV, photomultiplier tubes, can be operated linearly over large wavelength regions, are much more sensitive, are inherently freer of noise, and have much quicker response characteristics than the best solid state IR detectors. In addition they are more easily used in hostile environments, needing only electrical connections in contrast to quality IR detectors which require cryogenic or high-pressure gas systems. Visible-ultraviolet optical materials, in general, can withstand strain and thermal shock better and transmit or reflect greater wavelength ranges than the corresponding IR materials.

The most significant advantage of V-UV technology over IR technology is the virtual absence of thermal (blackbody) radiation interferences in V-UV spectroscopy. In hot systems thermal interferences often limit the usefulness of IR measurements and complicate data reduction.

For these reasons the possibility of developing an *in situ* technique employing V-UV technology was investigated. Unfortunately, none of the major hydrocarbon species absorbs or emits radiation in the visible or accessible ultraviolet (wavelengths longer than 2,000Å). However, the radical species CH emits a strong band centered at 4,315Å. It is well documented that CH radicals are present in the flames of CH_4 and other simple hydrocarbons (Ref. 20). In a CH_4-air flame stabilized on a flat flame burner it has been established that all the CH_4 has been destroyed in the luminous region of the flame (Ref. 21). This flame is a good system for the testing of CH emission as a function of fuel-to-air ratio and height above the burner.

6.1 EXPERIMENTAL DETAILS

A water-cooled, brass 7.6-cm-diam flat flame burner was used for this preliminary study. The experimental system is shown schematically in Fig. 22. A dove prism was positioned in front of the vertical slit of a 0.75-m spectrometer to rotate the image of the flame to allow sampling of the radiation from a horizontal section of the flame. The spectrometer slits were set at 50 μ, which gave a resolution of 0.5Å.

6.2 RESULTS AND DISCUSSION

Flames of equivalence ratio (ϕ) 1.2, 1, and 0.87 were studied. The most prominent spectral feature observed was the piled-up Q branch of the $^2\Delta \rightarrow {}^2\pi$ electronic transition at 4,315 Å.

18

This region of the spectrum for the ϕ = 1.0 flame with the optical path just above the surface of the burner is shown in Fig. 23. For the three flames under these conditions (ϕ = 1.2, 1, and 0.87) the relative heights of the peak at 4,313Å are 1.00, 0.46, and 0.22, revealing the expected trend that CH emission is greater in richer flames. At 5 mm above the burner surface, however, no CH emission was observed.

These observations indicate that CH emission and the CH_4 content of these flames are correlated. However, the function relating the two quantities was not determined. This function will be very strongly related to the temperature and the chemical composition of the system.

CH emission might be a useful field-monitoring technique for previously characterized high-temperature systems, used to detect changes in hydrocarbon emissions and temperature. It does not appear, however, that it would be a useful technique for an *in situ* diagnostic technique because of the calibration problems and the strong temperature dependence.

7.0 PROBE SIMULATOR EXPERIMENT

One of the ultimate objectives of this program is to develop a technique to evaluate the ability of probe technology to maintain the chemical integrity of the hydrocarbon constitutents of drawn samples from a hot gas stream. Recent studies (Refs. 1, 2, 3, 4, and 5) present considerable evidence that NO and CO concentrations in a hot gas stream can be significantly altered by the probing process. A probe simulator was built and used to study these effects. The simulator was designed for studying the effects of the hot internal probe surfaces on the chemical composition of sampled gases. Simulation of external flow-field effects was not addressed.

7.1 EXPERIMENTAL DETAILS

The probe simulation aparatus has been described previously (Ref. 2) and is shown in Fig. 24. It consists of a stainless steel tube, a Chromel®-Alumel® thermocouple, and a stainless steel plenum. A welding machine power supply was connected across the tube inlet. The thermocouple was attached to the outside surface of the tube between the welder connections to monitor the temperature. The gases to be investigated were introduced through the plenum and after passing through the probe were fed into an FID detector (Beckman Model 402) and a nondispersive IR CO_2 detector (Beckman Model 315A).

A mixture of gases was prepared to simulate the composition of a typical exhaust stream. It consisted of 7.2 percent CO_2, 12 percent O_2, and 110.8 ppm CH_4 in N_2. This mixture was introduced at ambient temperature and pressure. The temperature of the tube

inlet was then raised by increasing the current flow from the welding machine. A probe tip temperature versus gas sample concentration was then recorded.

7.2 RESULTS AND DISCUSSION

Probe tip temperatures ranging from ambient to 783°K were obtained. The gas temperature in the probe was not measured, but significant heating of the gas probably did not occur except at the internal probe surfaces. Carbon dioxide and THC content were monitored at all probe tip temperatures. No changes in either were detected at any temperature. These results indicate that hydrocarbons might be less susceptible to destruction in a probe than would NO or CO, which showed marked changes when this apparatus was used (Ref. 2).

8.0 COMBUSTOR EXPERIMENTS

Attempts were made to detect CH_4 and THC content in the ETF R-2C-1 research test area combustor with *in situ* optical measurement, optical measurements of drawn samples, online analysis of drawn samples, and laboratory analysis of drawn samples.

8.1 APPARATUS AND PROCEDURES

The R-2C-1 combustor facility is described in detail elsewhere (Ref. 2) and is shown in Fig. 25. An AVCO-Lycoming cylindrical combustor (14-cm diameter) is housed in a 40.6-cm-diam plenum section. The combustor exhausts into the test section through a standard ASME long radius convergent nozzle having an exit diameter of 5.5 cm. For the present test, a pressure-controlled tank supplied JP-4 fuel to the combustor, and the flow was measured by two turbine flowmeters. The plenum was connected to a controlled secondary airflow system and was operated at pressures slightly less than atmospheric by means of the ETF exhausters. The test section contains optical viewing ports on both sides. Mounted below the test section is a moveable yoke with mounting plates. The *in situ* optical devices, a source and receiver, were mounted on the plates. A multiprobe rake was located in the test section so that the probe entrance plane coincides with the optical path. The rake contains a stainless steel, orifice-type probe (Fig. 26), a thermocouple probe, and a cone pressure probe.

Samples, collected with the orifice-type probe, were pumped to the gas analyzer instruments by a bellows pump. This flow could also be diverted to fill containers to a pressure of 138 kPa. After the lines were purged with exhaust gas, the previously evacuated containers were opened to the stream. The 50.7-cm quartz cell described in Section 3.1 and an 86-cm-long, 10-cm-wide quartz cell used in the absorption experiments as well as 500-cc chemistry laboratory bottles were filled in this manner.

20

The laboratory bottle samples were analyzed with two instruments: an FID detector and a gas chromatograph apparatus capable of analyzing for CH_4.

Two spectroscopic instruments were used for the *in situ* measurements: a 0.25-m grating spectrometer and an AEDC EOCOM interferometer. The spectrometer slits were set at 200 μ, resulting in a bandpass of about 10 cm^{-1}. The spectrometer was equipped with a cooled InSb detector. The interferometer, described in Section 3.1, was also used in the laboratory absorption studies of the drawn samples.

The *in situ* measurements were attempted at the combustor nozzle exit. The diameter of the plume and hence the pathlength was 5.5 cm, and the static temperature was calculated by the method of Ref. 22 to be $1,230°K$.

8.2 RESULTS AND DISCUSSION

No IR absorption of methane or any other hydrocarbons in the range from 2,800 to 3,250 cm^{-1} was observed in the *in situ* or the absorption cell experiments using either the spectrometer or the interferometer. These results are in agreement with the calculated detectability limits of Section 3.3 and the results of the online FID analysis and the laboratory gas chromatographic and FID analyses of the drawn samples.

The hydrocarbon laboratory results and the online analysis of the exhaust gases are presented in Table 4. The minimum detectability of CH_4 for the laboratory gas chromatographic analysis is 3 ppm. The fact that the THC measurements do not decrease downstream as do all other minor species due to the mixing of the plume with entrapped air suggests that these measurements are not reliable. A possible reason for this apparent discrepancy is that the probe-sampled gas might have been contaminated by hydrocarbon deposits baking off of the heated transfer lines from the probe.

The lower values of the measured THC concentration of the laboratory analyses relative to the online analyses indicates a problem with one or both of the measurement techniques. This apparent discrepancy may be due to the absorbing of small amounts of the hydrocarbons on the unheated walls of the sample bottles and/or the dissolving of small amounts of the hydrocarbons in condensed water vapor in the sample bottle. In addition, possible differences in operation and/or calibration of the FID detectors used in the measurements might account for some of the discrepancy.

9.0 CONCLUSIONS AND OUTLOOK FOR FUTURE WORK

An investigation was conducted to determine the feasibility of developing an *in situ* optical gaseous hydrocarbon analytical technique suitable for jet engine exhaust diagnostics. The techniques investigated were interferometric spectroscopy in the 2,800- to 3,250-cm^{-1}

region of the IR. absorption of the radiation of a modified He-Ne laser emitting in the IR, and CH visible emission spectroscopy. In addition to these studies the microwave-excited emission of methane, a candidate for use as a radiation source for correlation spectroscopy, was investigated. A related experiment, the simulation of the effect of probing on the hydrocarbon content of methane containing simulated exhaust gases, was also performed. A preliminary investigation of the hydrocarbon content of the exhaust of a combustor in the ETF R-2C-1 test cell was also reported. A brief discussion of these items follows.

The interferometric absorption spectra of methane in nitrogen at concentrations from 100 to 1.000 ppmv, at temperatures from 297 to 773°K at a total pressure of 97.9 kPa were recorded and analyzed within a curve of growth calculational framework. It was found that individual methane absorption lines could be modeled using available literature spectral parameters, providing proper account is taken of the thermal depopulation of the absorbing state. This modeling provided the means of calculating methane detectability limits as a function of temperature and pathlength assuming that 6-percent absorption is the limit of detectability in a test environment. Total hydrocarbon content detectability limits were estimated in a similar manner.

Absorption spectra of heptane in nitrogen at a concentration of 500 ppmv at temperatures from 297 to 773°K were recorded. No line structure was observed, but the data were analyzed to give molecular absorption coefficient information.

A specially modified He-Ne laser source multiple pass absorption system was developed. This system attained 36-pass operation, but signal stability problems must be overcome before absorption measurements can be made.

The microwave-excited IR emission of methane was recorded interferometrically and was found to be very weak, and unsuitable for use as a resonance radiation source. CH visible emission spectra of methane-air flames were recorded and found to be correlated to the methane content of the flames. Simulation of mechanical probing for the detection of methane contained in a simulated exhaust gas at temperatures from ambient to 783°K did not alter the hydrocarbon concentrations.

No hydrocarbon IR absorption was detected in the combustor exhaust in the ETF R-2C-1 test cell in *in situ* measurements or in absorption cell measurements of drawn samples. These results are in agreement with FID analyses of drawn samples and detectability limit calculations. The FID analyses of the drawn samples and the online FID measurements, however, are thought to be unreliable.

It was concluded that the future development of IR absorption hydrocarbon detection is dependent upon the attainment of long pathlength and high resolution. The availability of narrow wavelength output, tunable diode lasers presents an attractive option if sufficient power can be provided by these lasers for multiple-pass applications. A tunable narrow wavelength output laser source can combine high resolution and long pathlength capabilities while eliminating the need for reference beams for monitoring laser power stability, degradation of optical components, and scattering by particulates. In addition, this high-intensity source eliminates the need for correction for both thermal emission and continuous absorptions of other species.

REFERENCES

1. Few, J. D., Bryson, R. J., and McGregor, W. K. "Evaluation of Probe Sampling versus Optical In Situ Measurements of Nitric Oxide Concentrations in a Jet Engine Combustor Exhaust." AEDC-TR-76-180 (ADA034726), January 1977.

2. Few, J. D., Bryson, R. J., and Lowry, H. S. III. "Optical In Situ versus Probe Measurements of Nitric Oxide Concentration as a Function of Axial Positions in a Combustor Exhaust." AEDC-TR-78-32.

3. Bryson, R. J. and Few, J. D. "Comparison of Turbine Engine Combustor Exhaust Emissions Measurements Using Three Gas Sampling Probe Designs." AEDC-TR-78-7.

4. Benson, R. and Samuelsen, G. S. "Oxides of Nitrogen Transformation While Sampling Combustor Products Containing Carbon Monoxide and Hydrogen." Presented at the 1976 Fall Meeting, Western States Section, Combustion Institute, University of California, San Diego, October 18-20, 1976.

5. Benson, R., and Samuelsen, G. S. "Oxides of Nitrogen Transformation While Sampling Combustion Products Containing Carbon Monoxide, Hydrogen, and Hydrocarbons." Presented at the 1977 Spring Meeting, Western States Section, Combustion Institute, University of Washington, Seattle, April 18-19, 1977.

6. Jackson, M. W. "Analysis for Exhaust Gas Hydrocarbons - Nondispersive versus Flame-Ionization." Journal of the Air Pollution Control Association. Vol. 11, 1966, pp. 697-702.

7. Conkle, J. P., Lackey, W. W., Martin, C. L., and Miller, R. L. "Organic Compounds in Turbine Combustor Exhaust." Presented at the International Conference on Environmental Sensing and Assessment, Las Vegas, Nevada, September 14-19, 1975.

8. Leonard, D. A. "Field Tests of a Laser Raman Measurement System for Aircraft Engine Exhaust Emissions." AFAPL-TR-74-100, October 1974.

9. Roquemore, W. M. and Hodgson, F. N. "Fluorescence of Hydrocarbons in Jet Engine Exhausts." Presented at the International Conference on Environmental Sensing and Assessment, Las Vegas, Nevada. September 14-19, 1975.

10. Lazalier, G. R. and Gearhart, J. W. "Measurement of Pollutant Emissions from an Afterburning Turbojet Engine at Ground Level: II: Gaseous Emissions." AEDC-TR-72-70 (AD747773), August 1972.

11. Davidson, D. L. and Domal, A. F. "Emission Measurements of a J93 Turbojet Engine." AEDC-TR-73-132 (AD766648), September 1973.

12. Mitchell, A.C.G. and Zemansky. M. W. Resonance Radiation and Excited Atoms. The MacMillan Company, New York, 1934.

13. Herzberg, G. Molecular Spectra and Molecular Structure II: Infrared and Raman Spectra of Polyatomic Molecules. D. Van Nostrand Company, New York, 1945.

14. Varanasi, P., Pugh, L. A., and Bangaru, B. R. P. "Measurement of Multiplet Intensities and Noble Gas-Broadened Line Widths in the ν_3-Fundamental of Methane." Journal of Quantitative Spectroscopy and Radiative Transfer, Vol. 14, 1974, pp. 829-838.

15. Varanasi, P. "Collision-Broadened Half-Widths and Shapes of Methane Lines." Journal of Quantitative Spectroscopy and Radiative Transfer, Vol. 11, 1971, pp. 1711-1724.

16. Penner, S. S. Quantitative Molecular Spectroscopy and Gas Emissivities. Addison-Wesley Publishing Co., Inc., Reading, Mass., 1959.

17. Castellan, G. W. Physical Chemistry. Addison-Wesley Publishing Co., Inc., Reading, Mass., 1964.

18. Lennert, A. E., Sowls, R. E., Belz, R. A.. Goethert. W. H., Bentley, H. T., Powell, H. M., Baily, A. B., and McCay, T. D. "Electro-Optical Techniques for Diesel Engine Research." AEDC-TR-77-17 (ADA039357), May 1977.

19. Gerritsen, H. J. "Tuned-Laser Spectroscopy of Organic Vapors." Published in the Proceedings of the Physics of Quantum Electronic Conference held in San Juan, Puerto Rico, June 20-30, 1965.

20. Gaydon, A. G. The Spectroscopy of Flames. Wiley & Sons, New York, 1957.

21. Kaskan, W. E. and Reuther, J. J. "Limiting Equivalence Ratio, Dissociation, and Self-Inhibition in Premixed, Quenched, Fuel-Rich Hydrocarbon/Air Flames." Presented at the Sixteenth Symposium (International) on Combustion, M.I.T., Cambridge, Mass, 1977.

22. Osgerby, I. T. and Rhodes, R. P. "An Efficient Numerical Method for the Calculation of Chemical Equilibrium in the H/C/O/N/A System." AEDC-TR-71-256 (AD741825), April, 1972.

AEDC
1901-77

Figure 1. Interferometer spectrometer and data acquisition system.
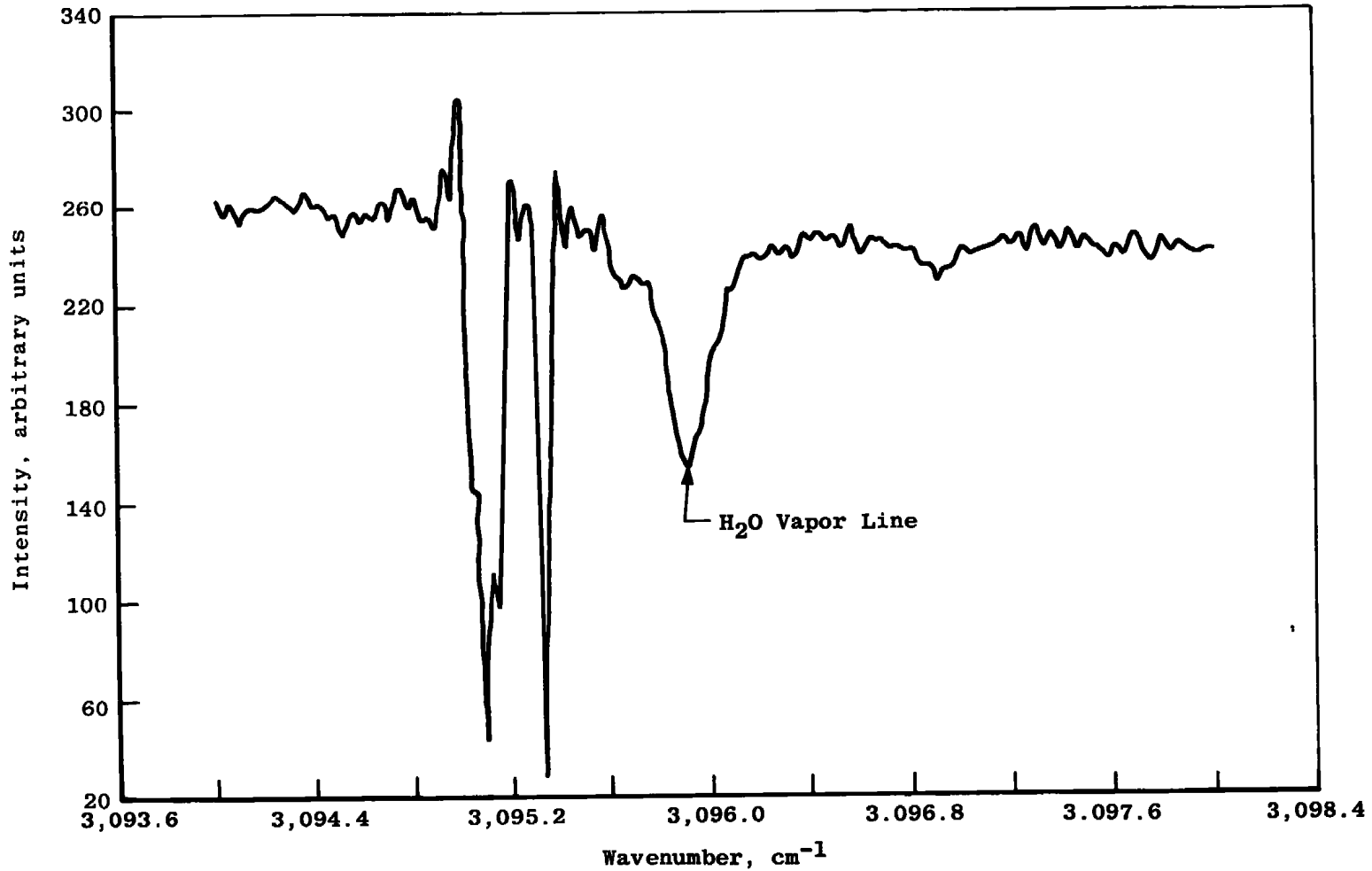
Figure 2. Absorption spectrum of methane at 297°K, R_7 line,
pressure 10.13 kPa, pathlength 7.5 cm.
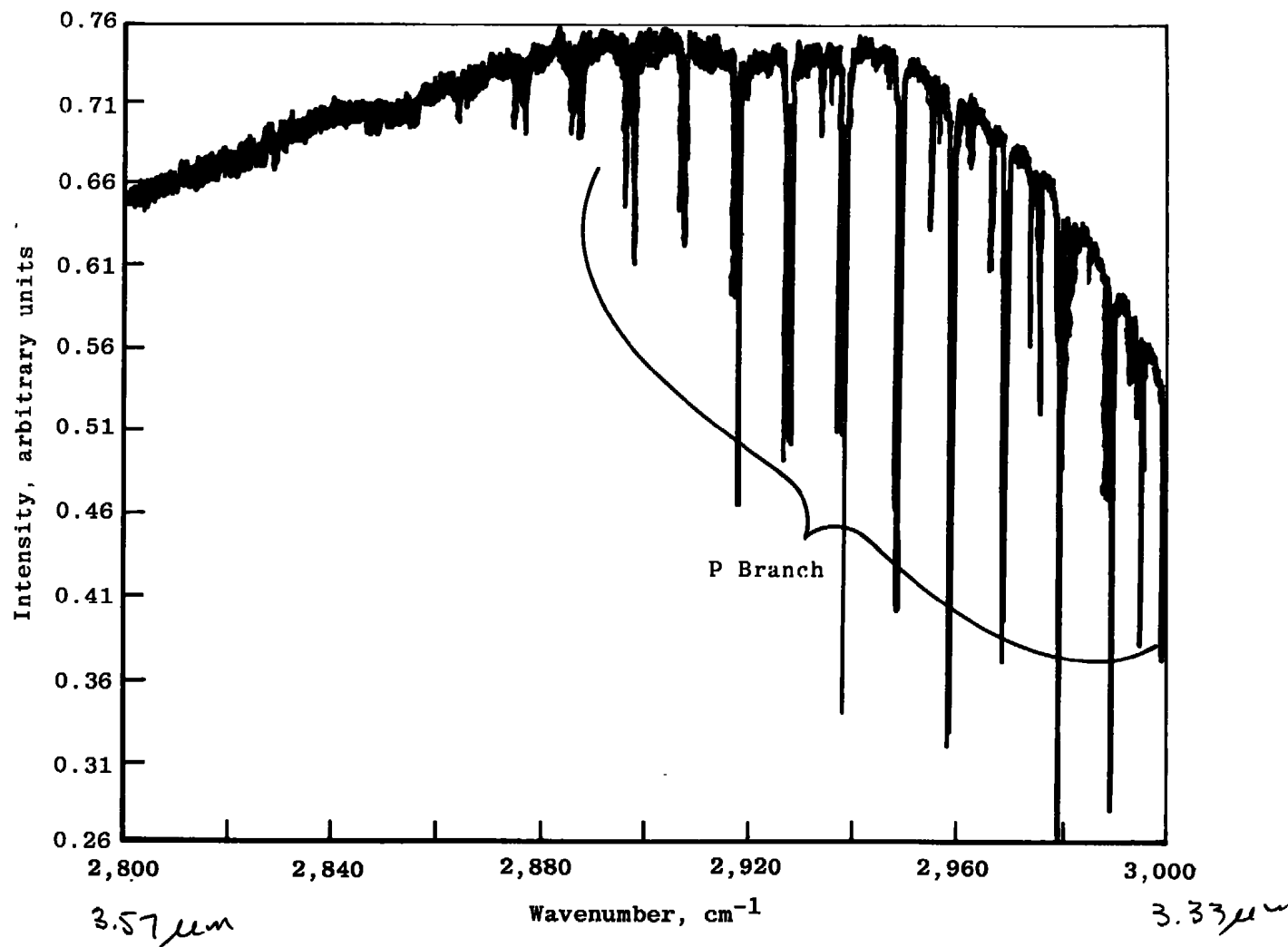
Figure 3. Absorption spectrum of methane in nitrogen at 297°K, methane concentration 996 ppm, pressure 97.9 kPa, pathlength 50.7 cm.
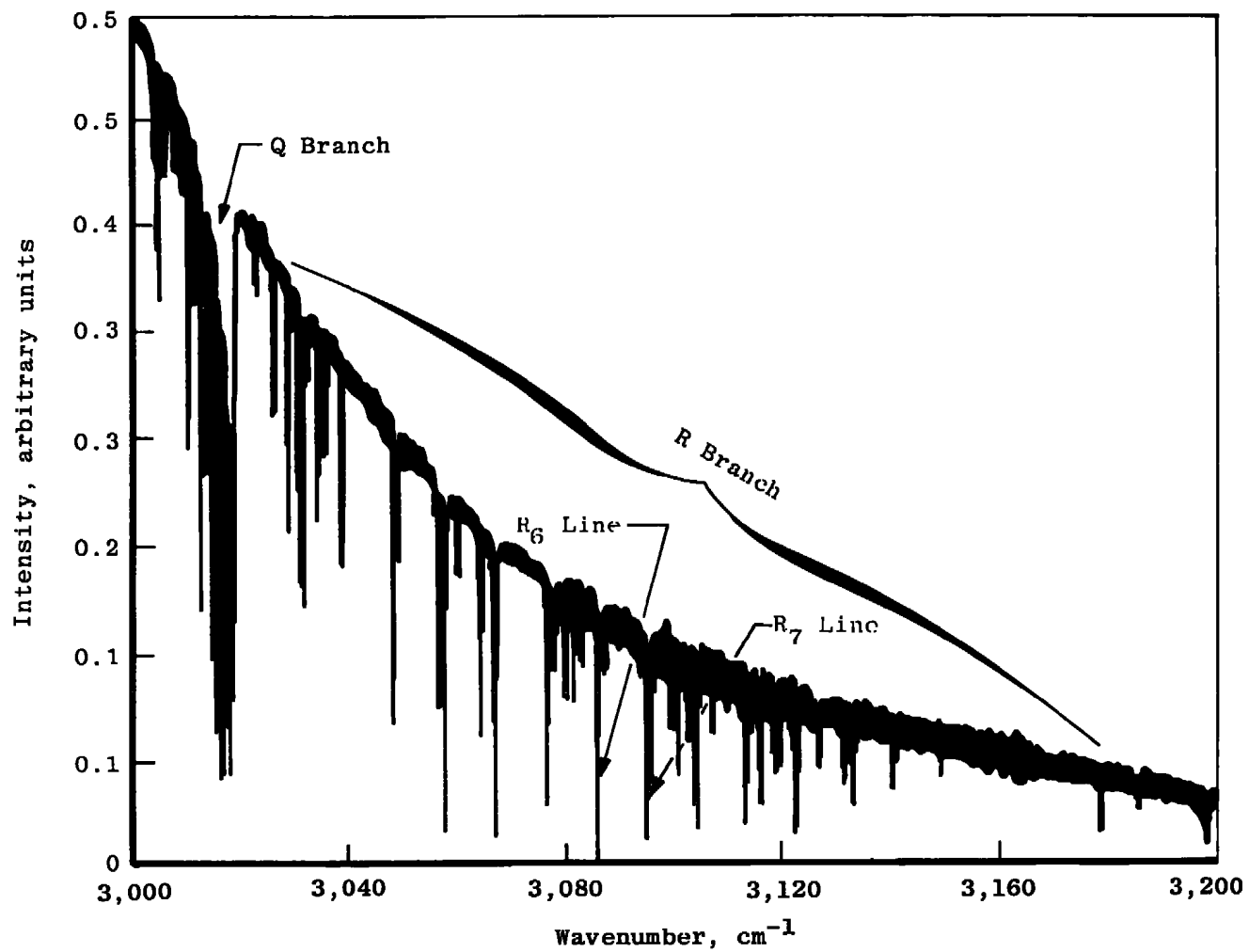
Figure 3. Concluded.
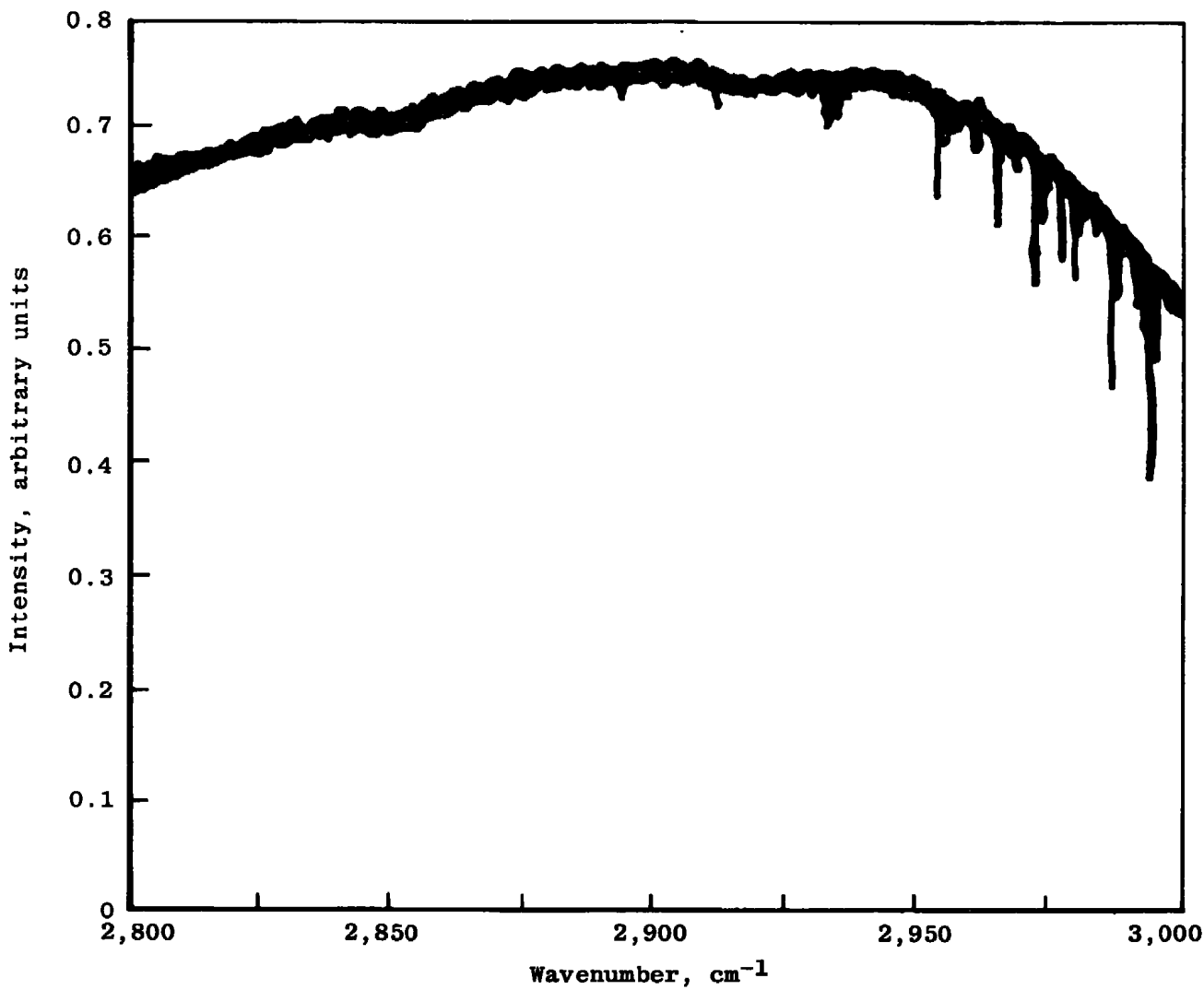
Figure 4. Empty cell spectrum, 297°K, pathlength 50.7 cm.
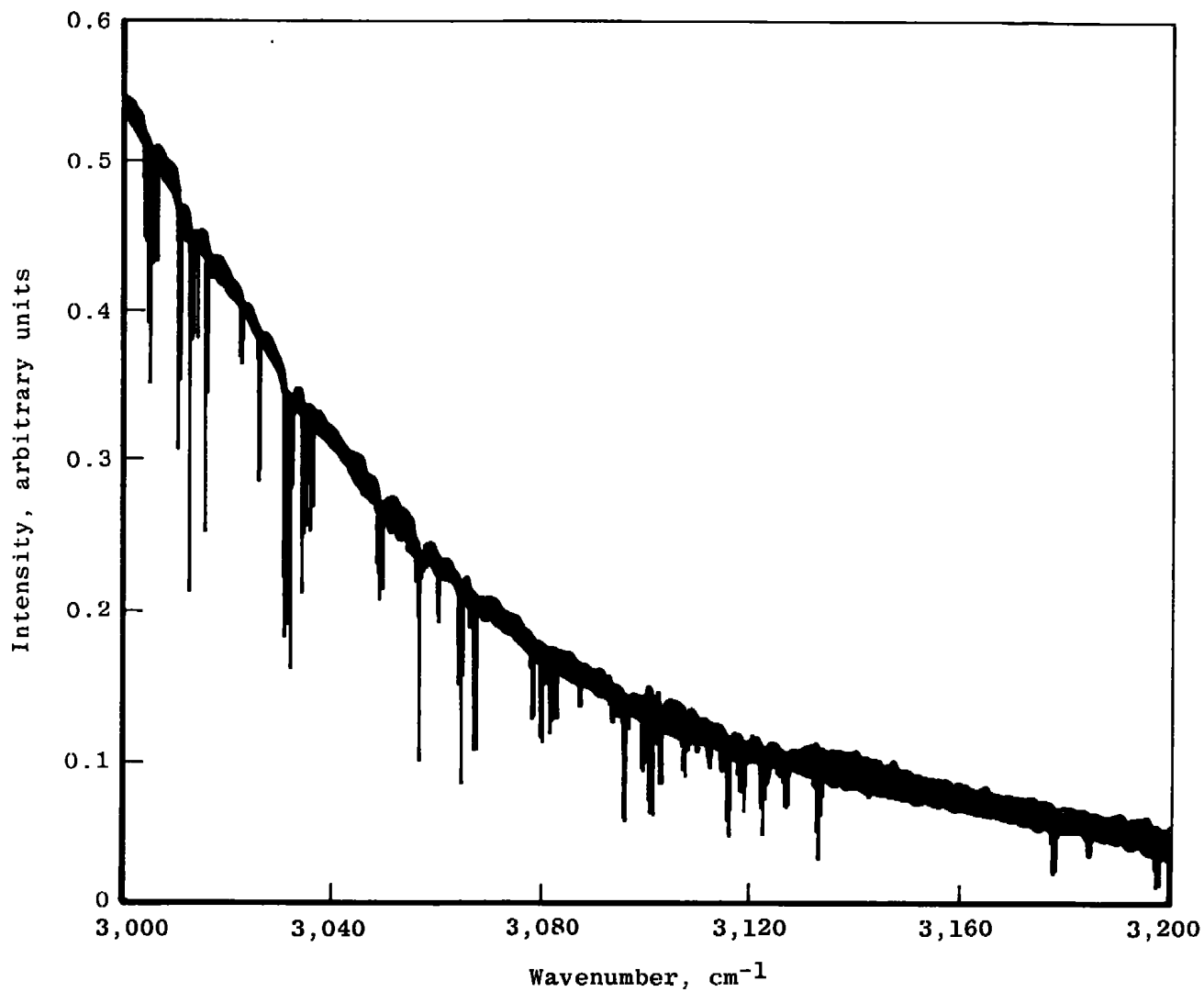
Figure 4. Concluded.
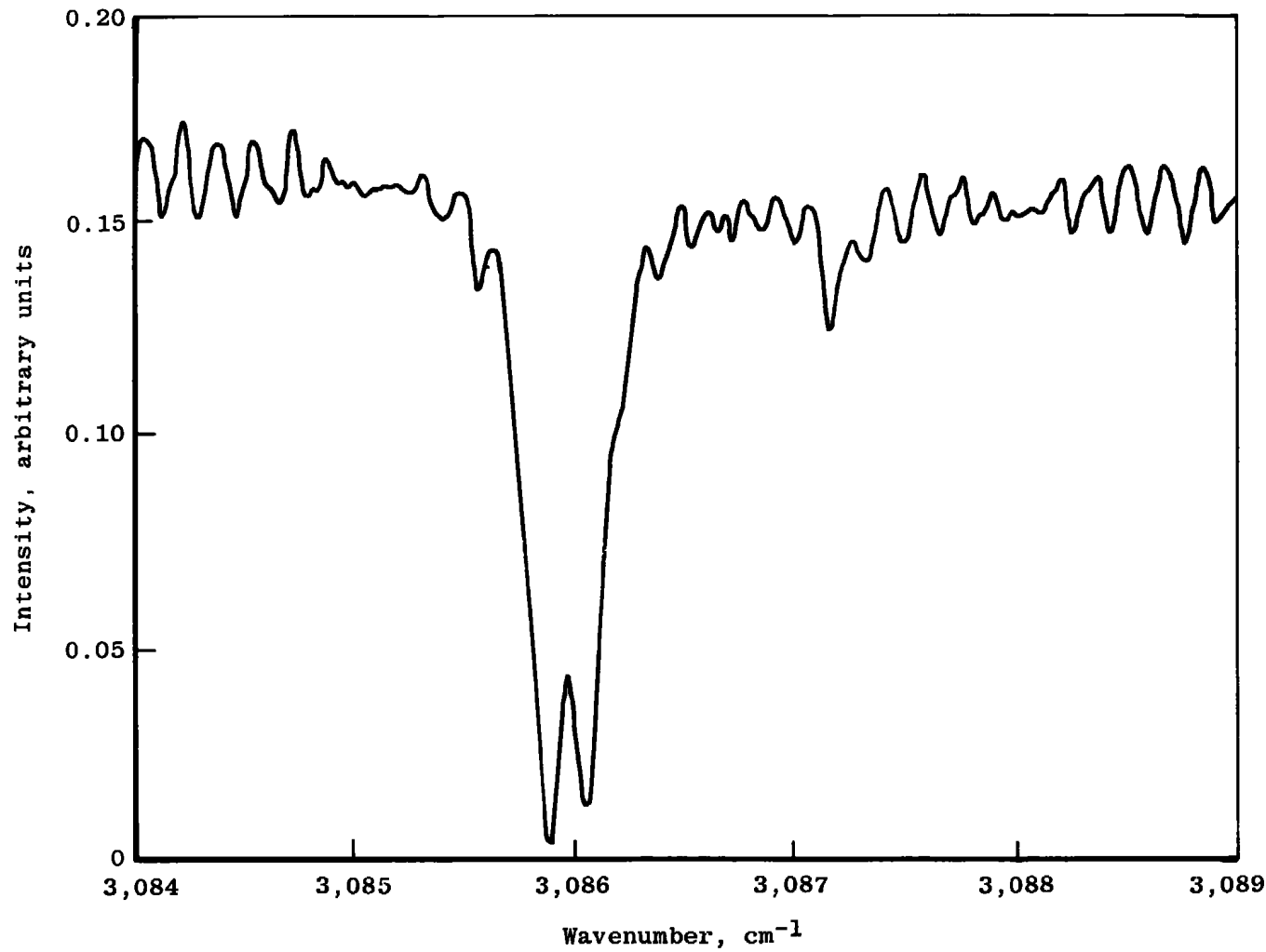
Figure 5. Absorption spectrum of methane in nitrogen at 297°K, R_6 line,
methane concentration 996 ppm, pressure 97.9 kPa, pathlength 50.7 cm.
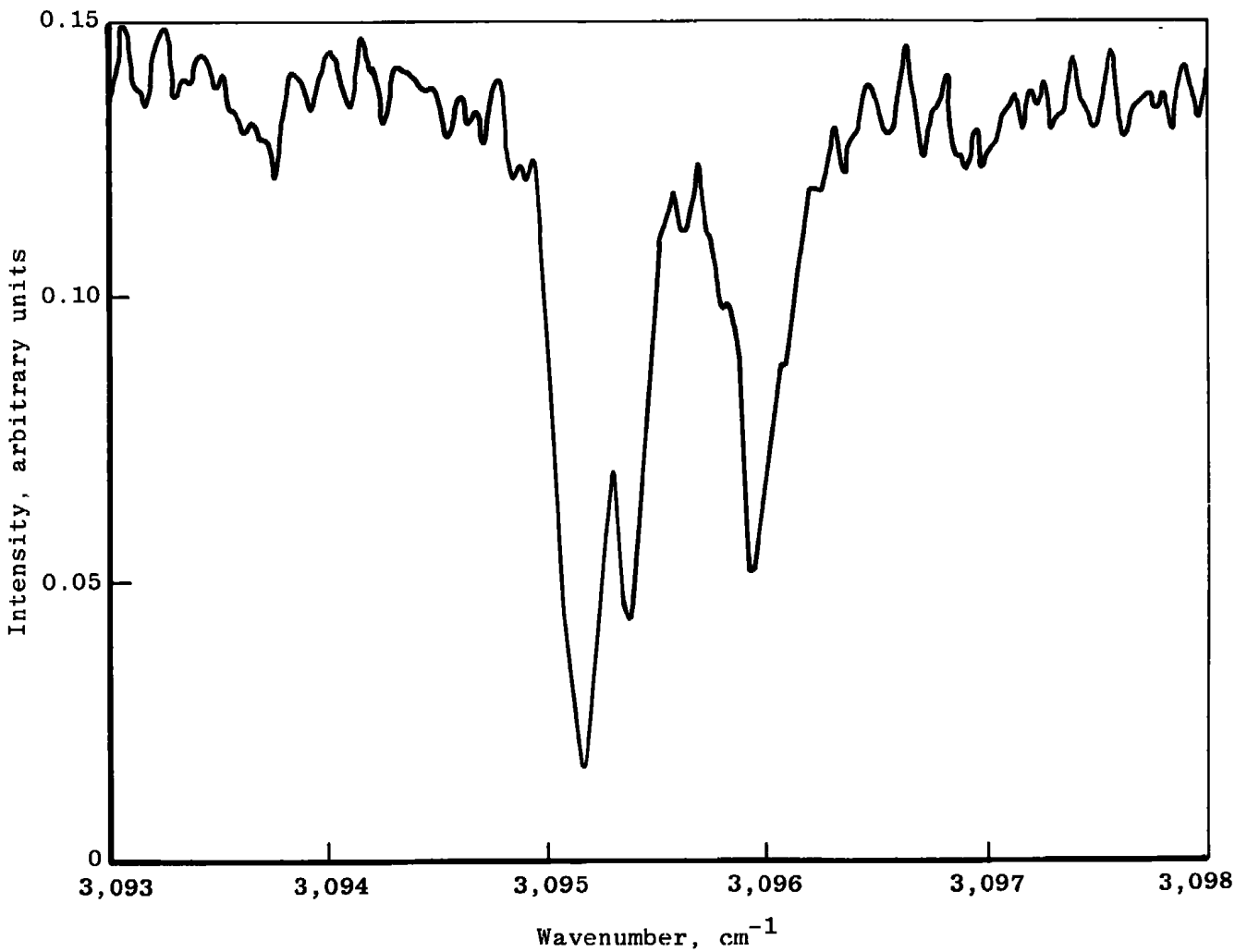
Figure 6. Absorption spectrum of methane in nitrogen at 297°K, R_7 line,
methane concentration 996 ppm, pressure 97.9 kPa, pathlength 50.7 cm.
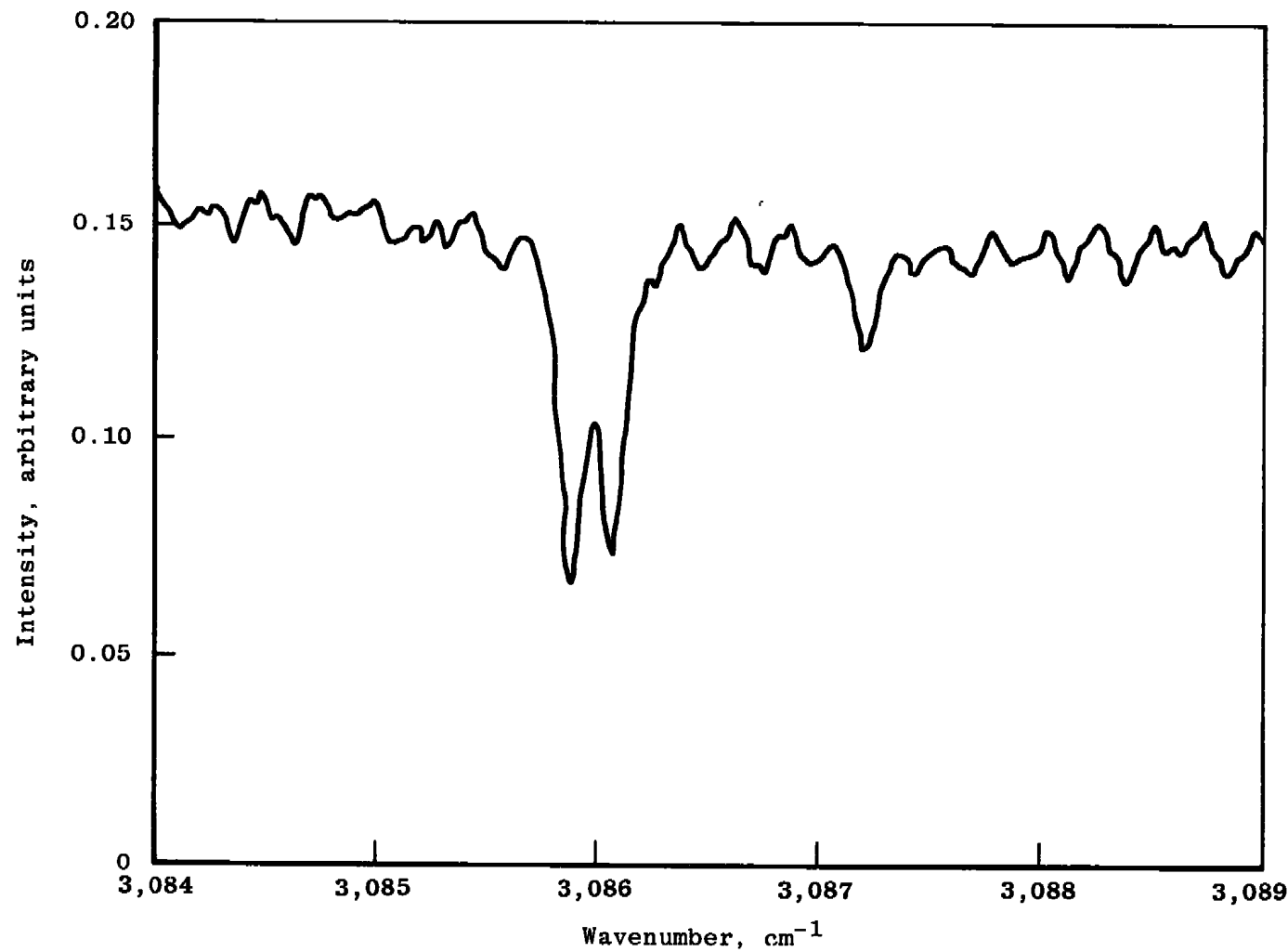
Figure 7. Absorption spectrum of methane in nitrogen at 573°K, R_6 line, methane concentration 996 ppm, pressure 97.9 kPa, pathlength 50.7 cm.
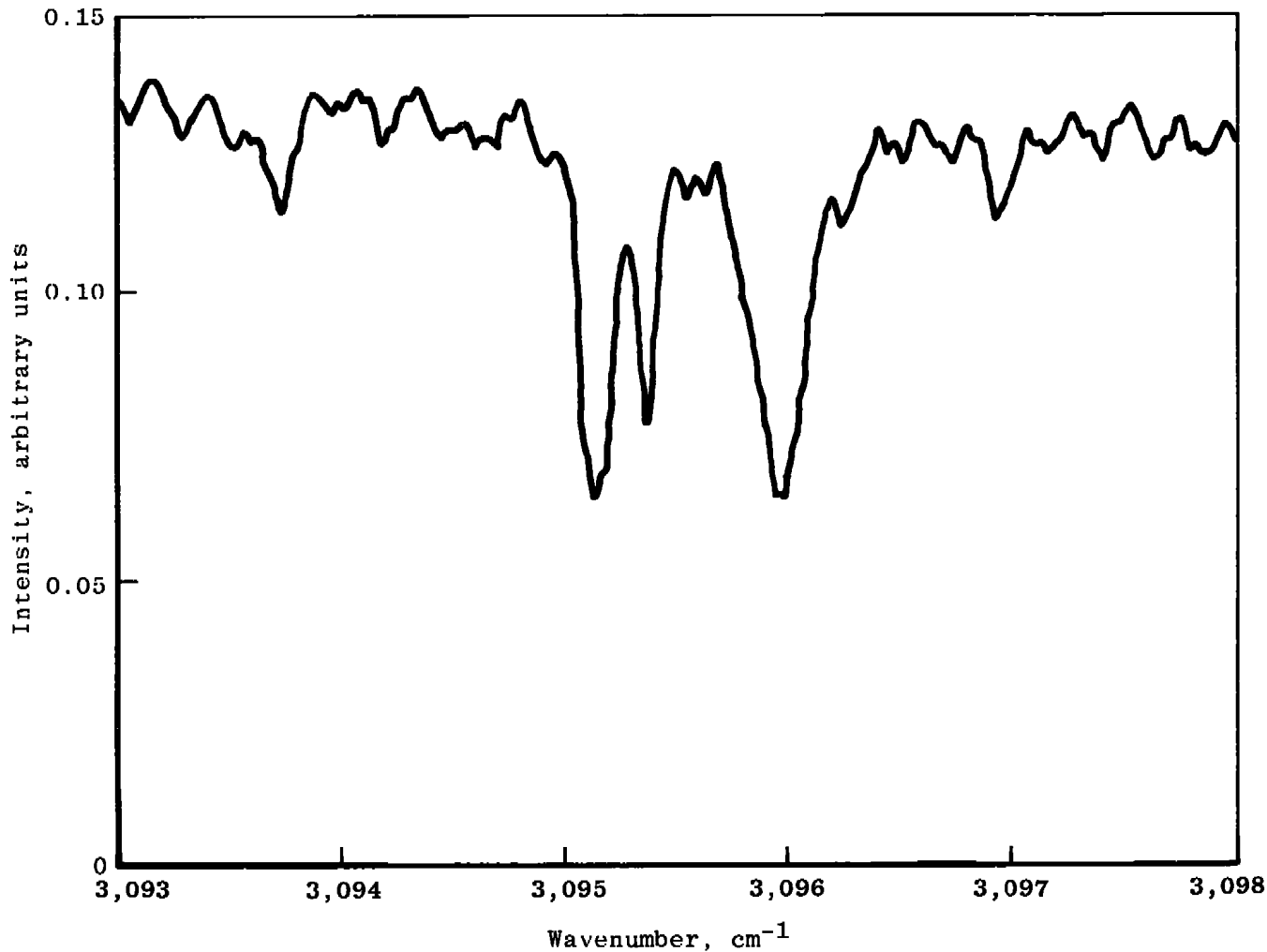
Figure 8. Absorption spectrum of methane in nitrogen at 573°K, R_7 line,
methane concentration 996 ppm, pressure 97.9 kPa, pathlength 50.7 cm.
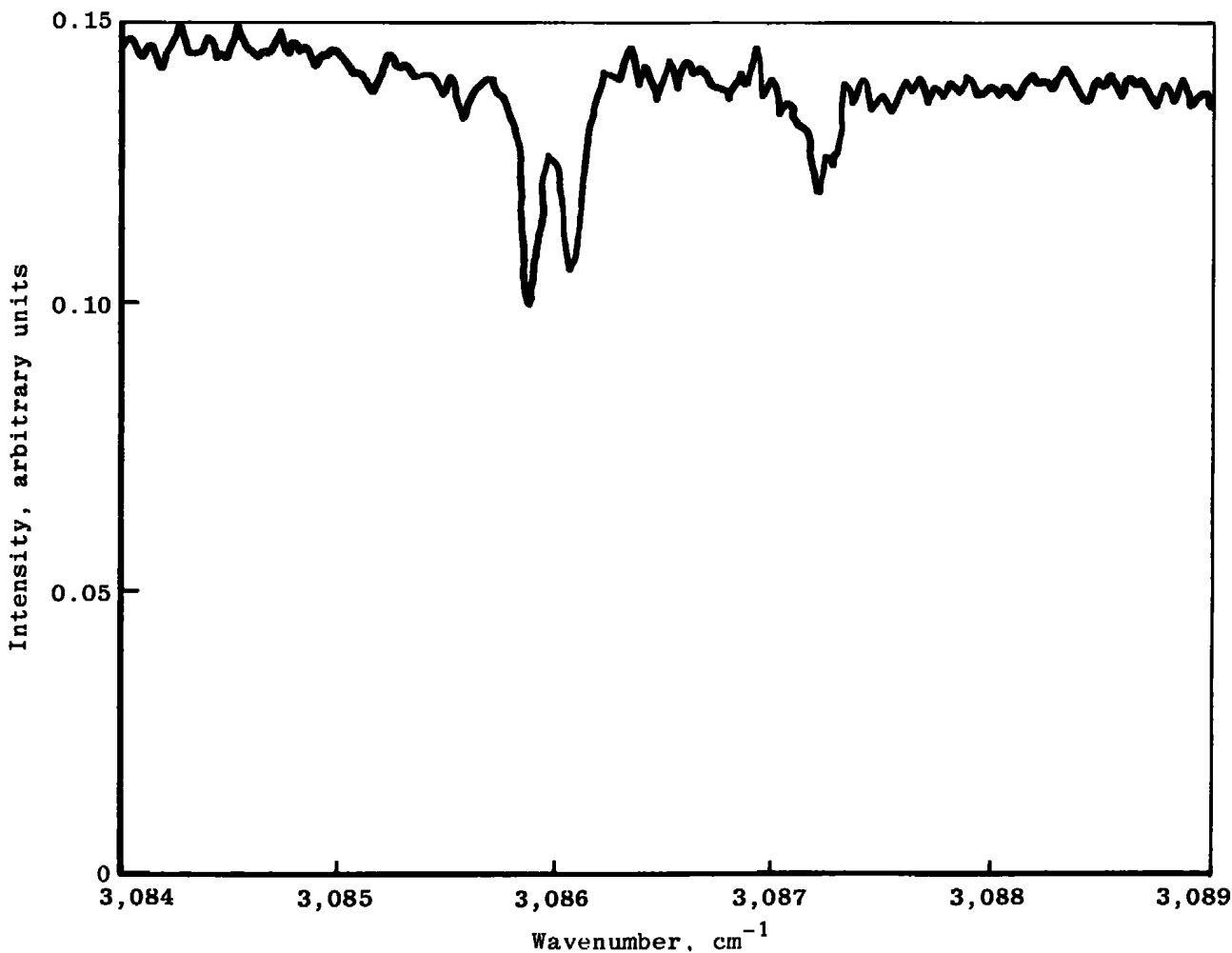
Figure 9. Absorption spectrum of methane in nitrogen at 773°K, R_6 line,
methane concentration 996 ppm, pressure 97.9 kPa, pathlength 50.7 cm.
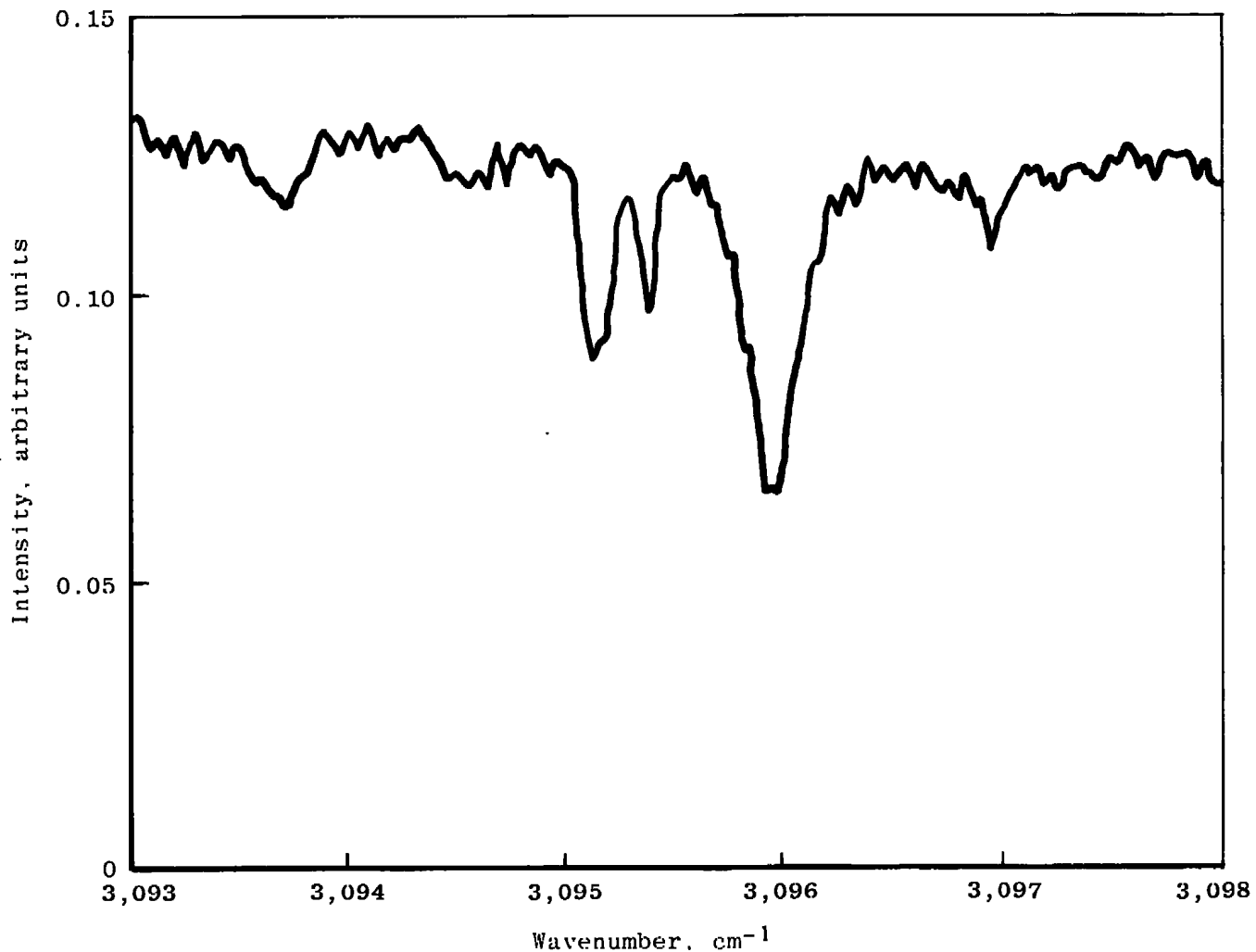
Figure 10. Absorption spectrum of methane in nitrogen at 773°K, R_7 line,
methane concentration 996 ppm, pressure 97.9 kPa, pathlength 50.7 cm.
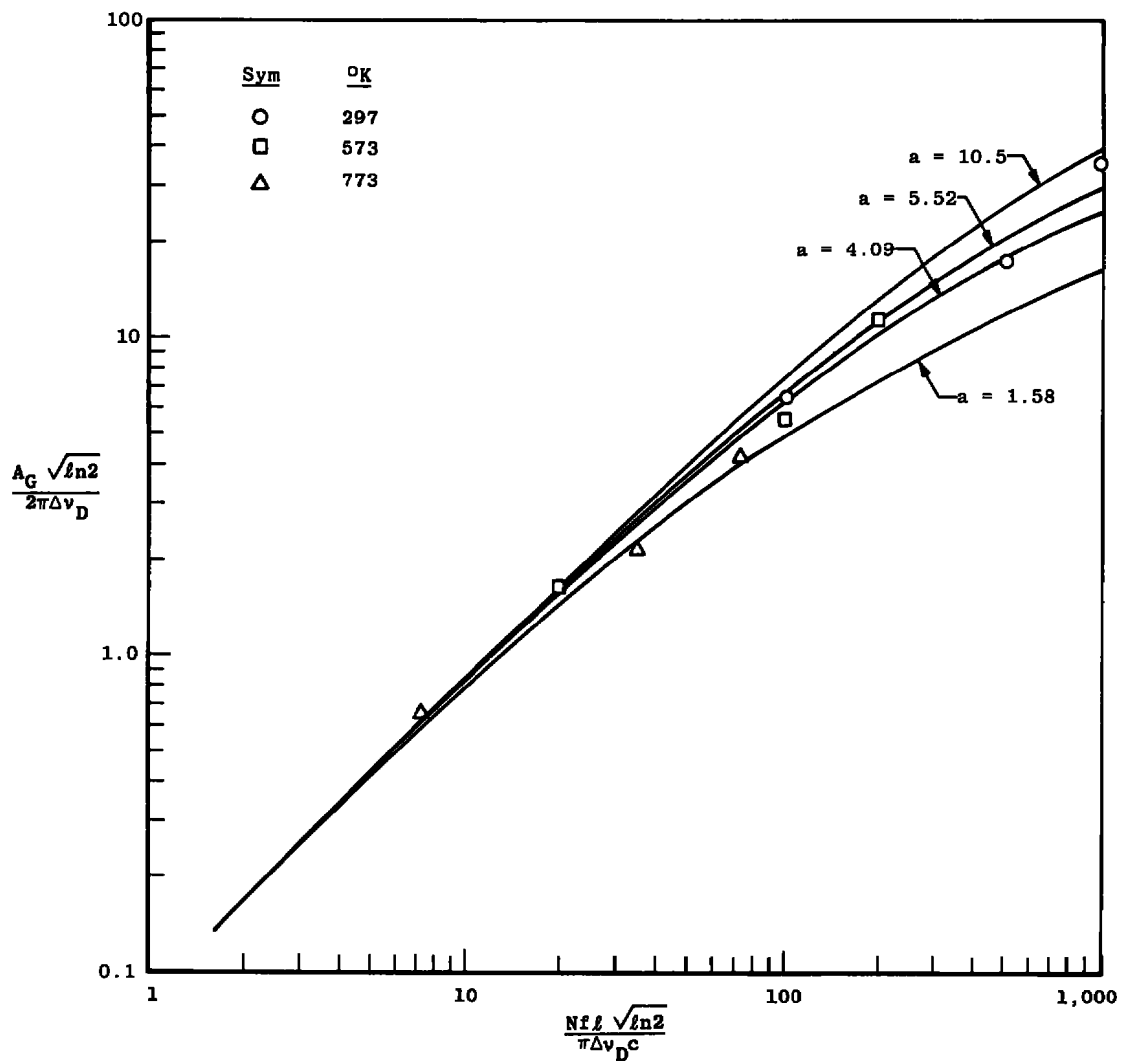
Figure 11. Curve of growth calculations and methane R_6 line data points.
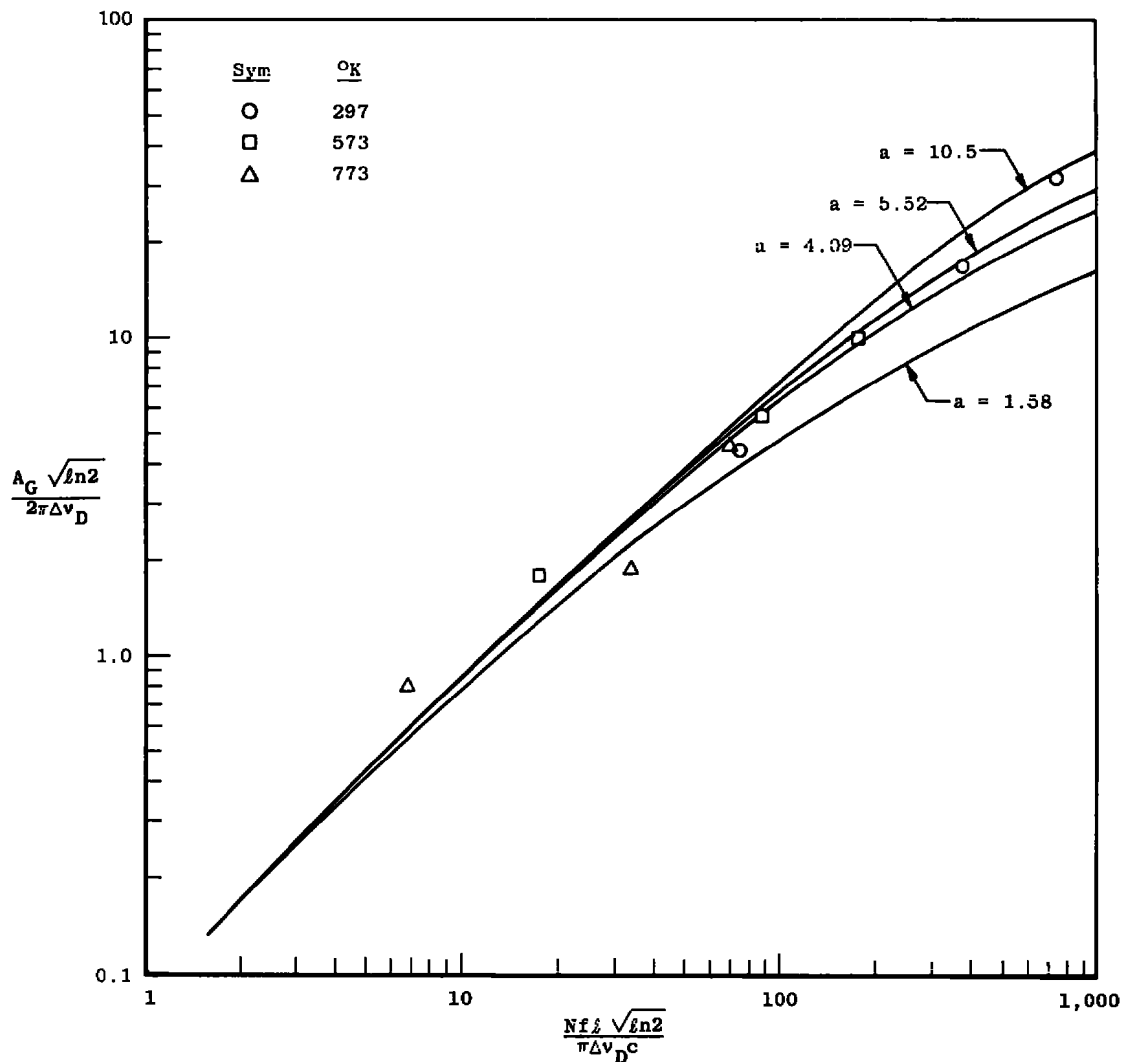
Figure 12. Curve of growth calculations and methane R7 line
data points.
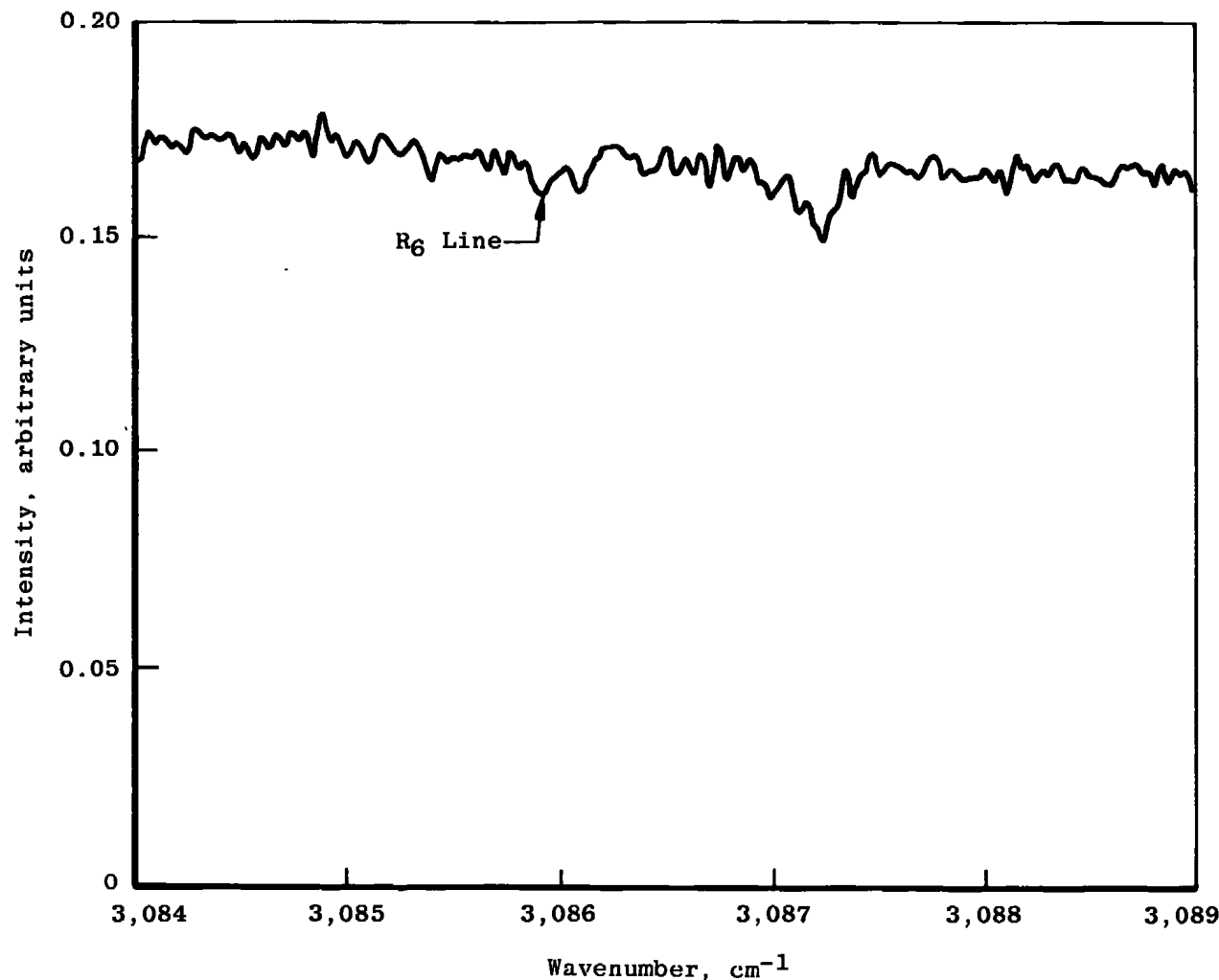
Figure 13. Absorption spectrum of methane in nitrogen at 773°K, R_6 line, methane concentration 99.6 ppm, pressure 97.9 kPa, pathlength 50.7 cm.
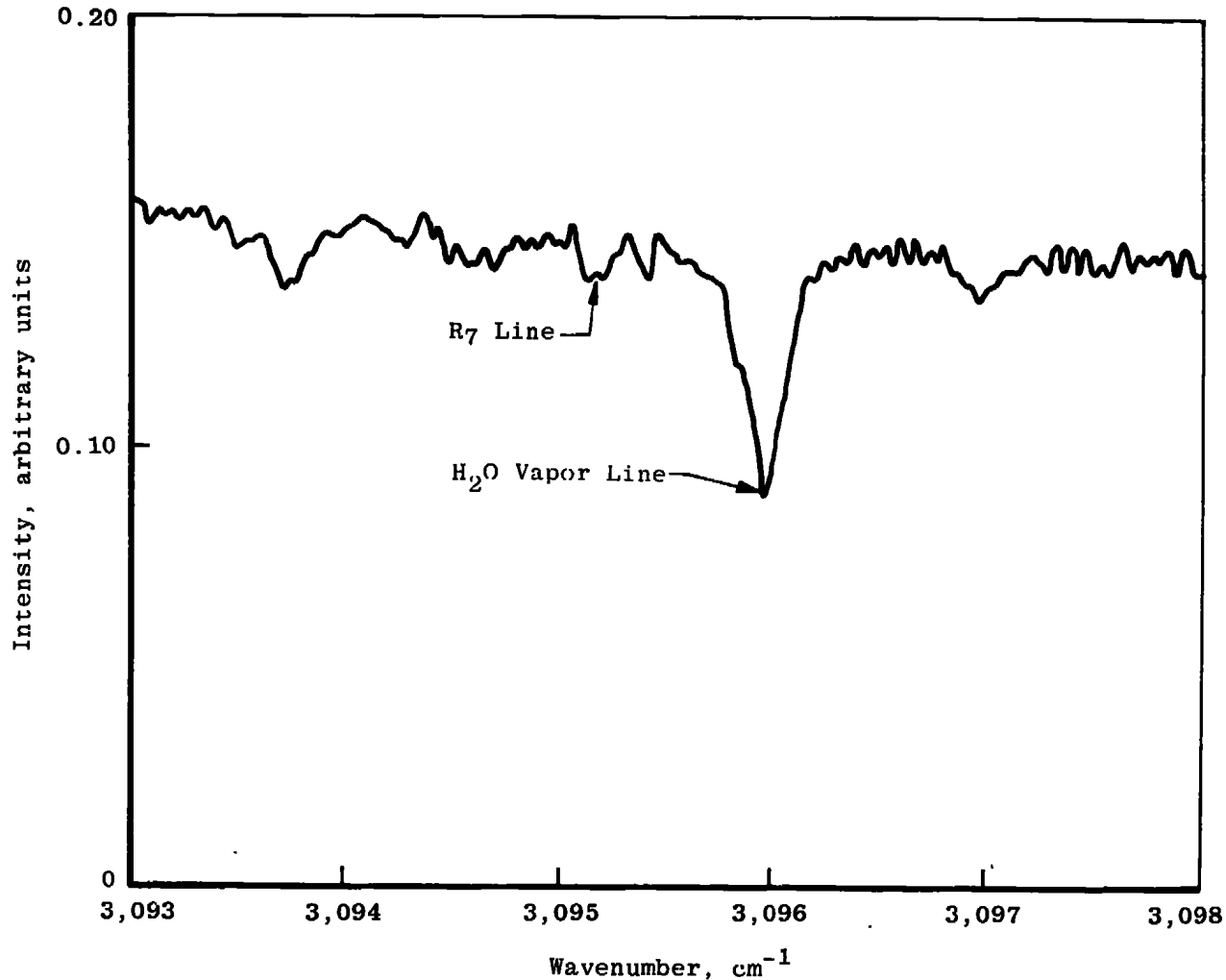
Figure 14. Absorption spectrum of methane in nitrogen at 773°K, R$_7$ line,
methane concentration 99.6 ppm, pressure 97.9 kPa, pathlength 50.7 cm.
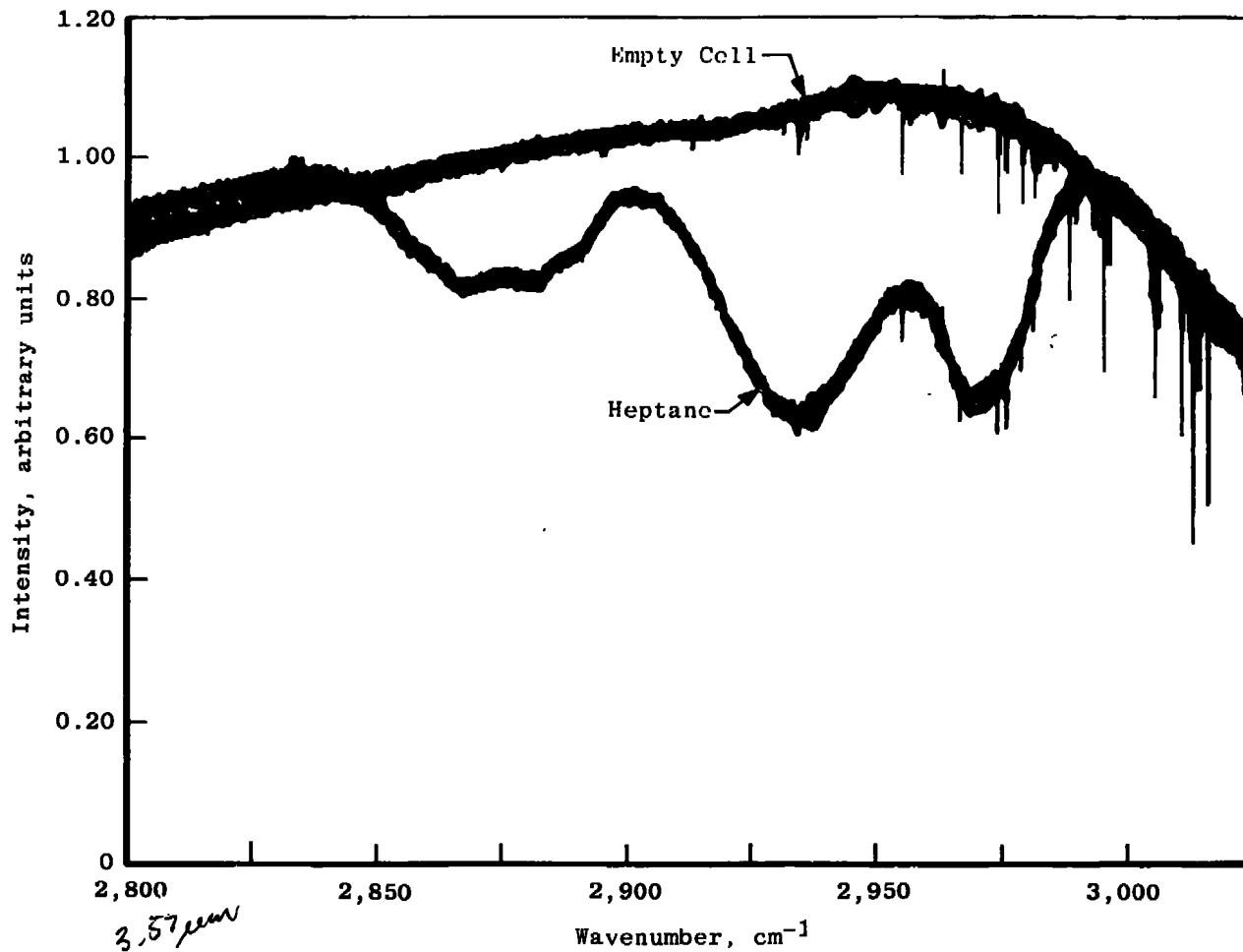
Figure 15. Absorption spectrum of heptane in nitrogen and empty cell spectrum
at 297°K, heptane concentration 516.8 ppmv, pressure 97.9 kPa,
pathlength 50.7 cm.
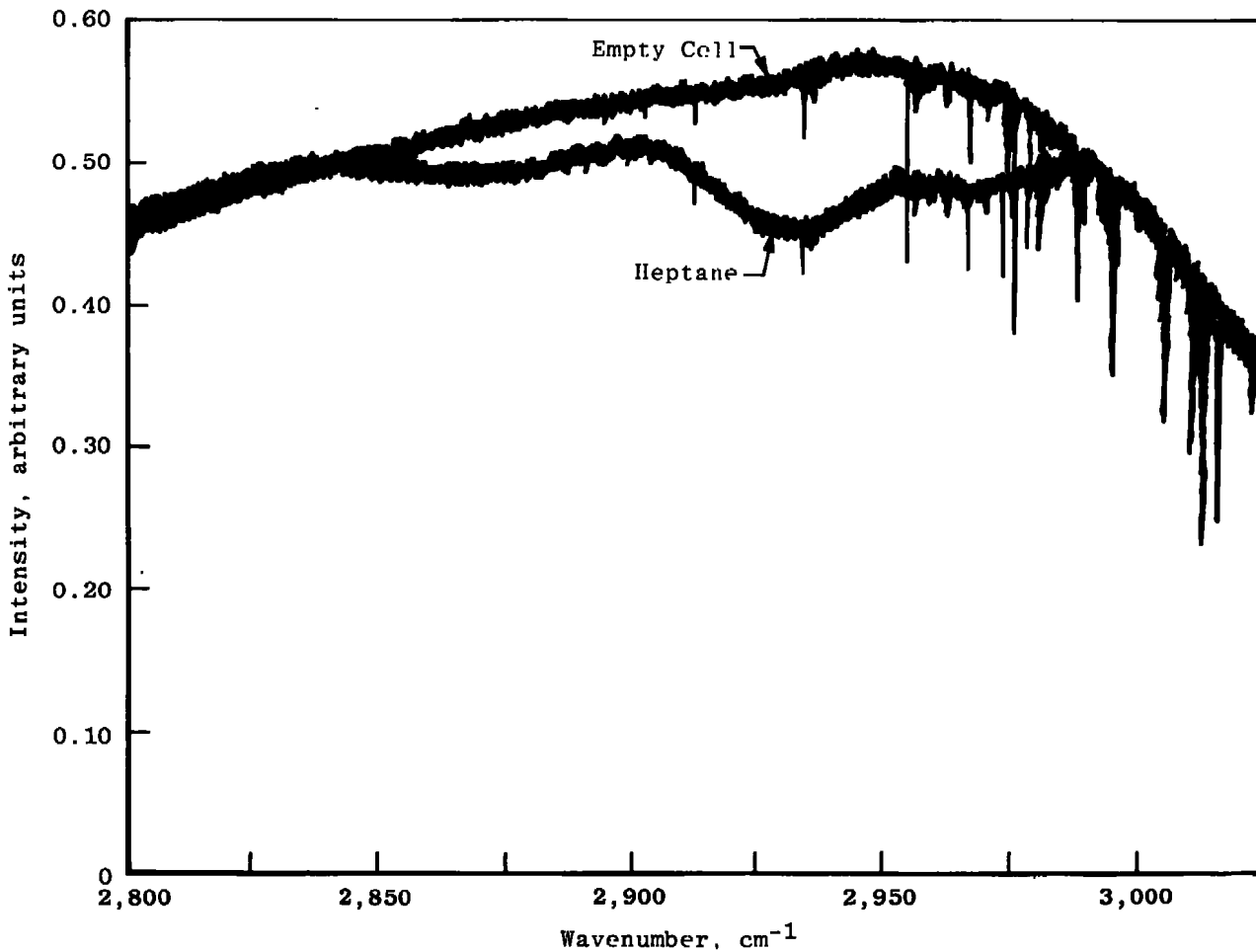
Figure 16. Absorption spectrum of heptane in nitrogen and empty cell spectrum at 573°K, heptane concentration 516.8 ppmv, pressure 97.9 kPa, pathlength 50.7 cm.
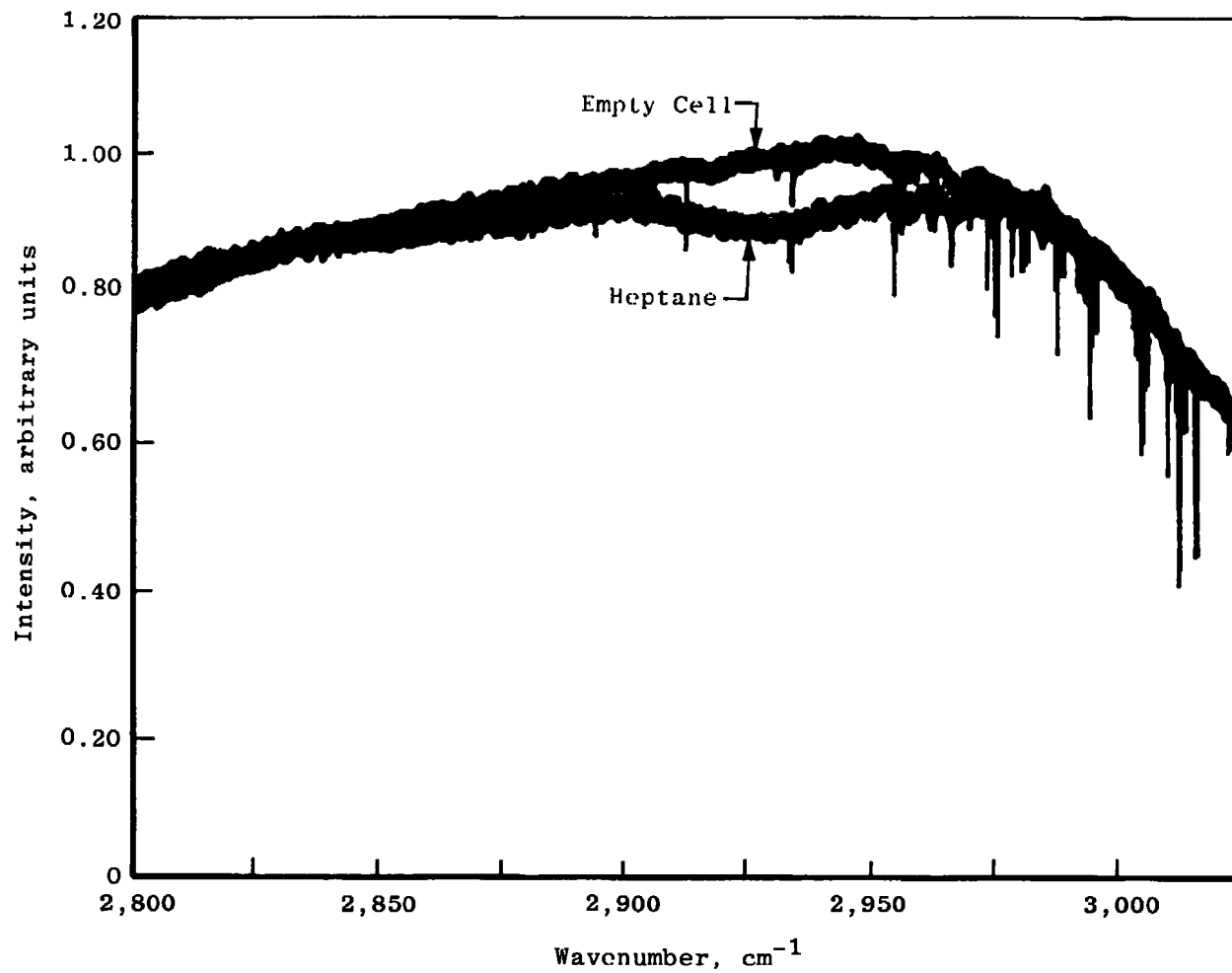
Figure 17. Absorption spectrum of heptane in nitrogen and empty cell spectrum at 773°K, heptane concentration 516.8 ppmv, pressure 97.9 kPa, pathlength 50.7 cm.
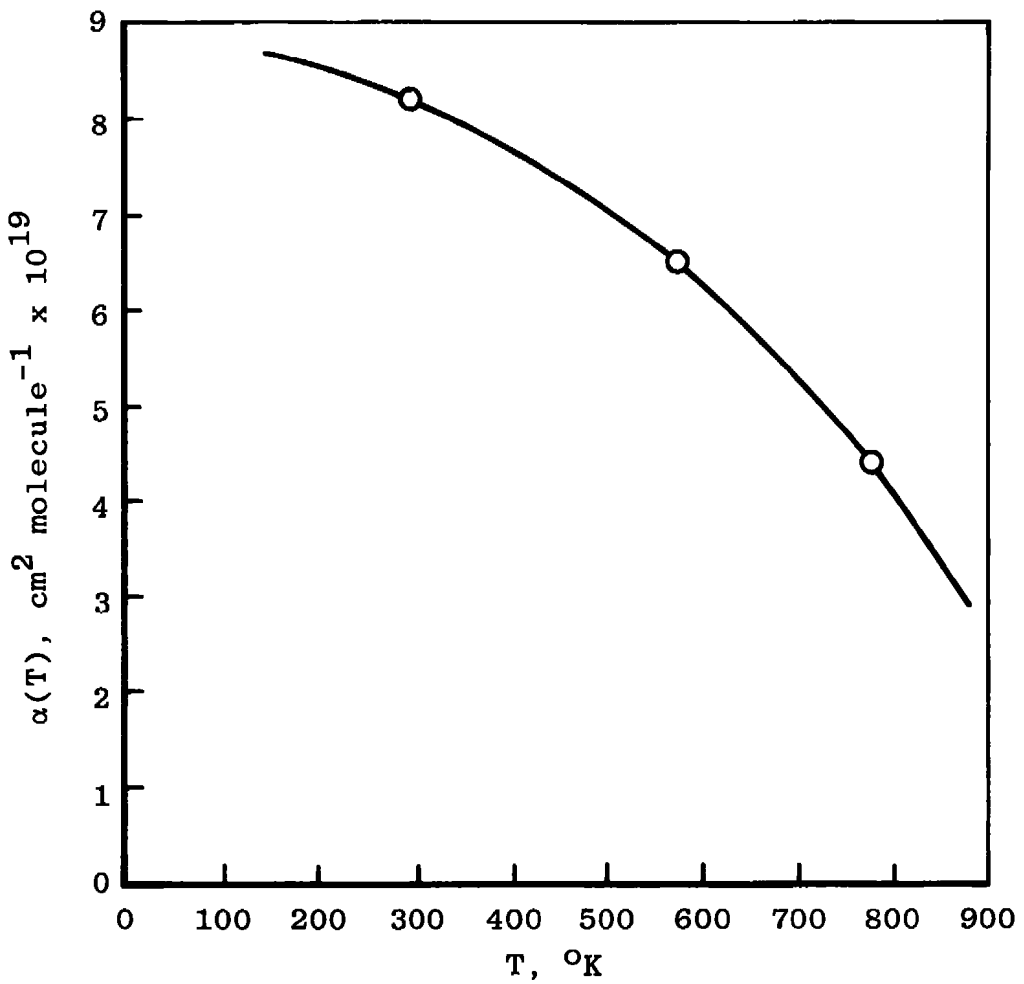
Figure 18. Heptane molecular absorption coefficient as a function of temperature.
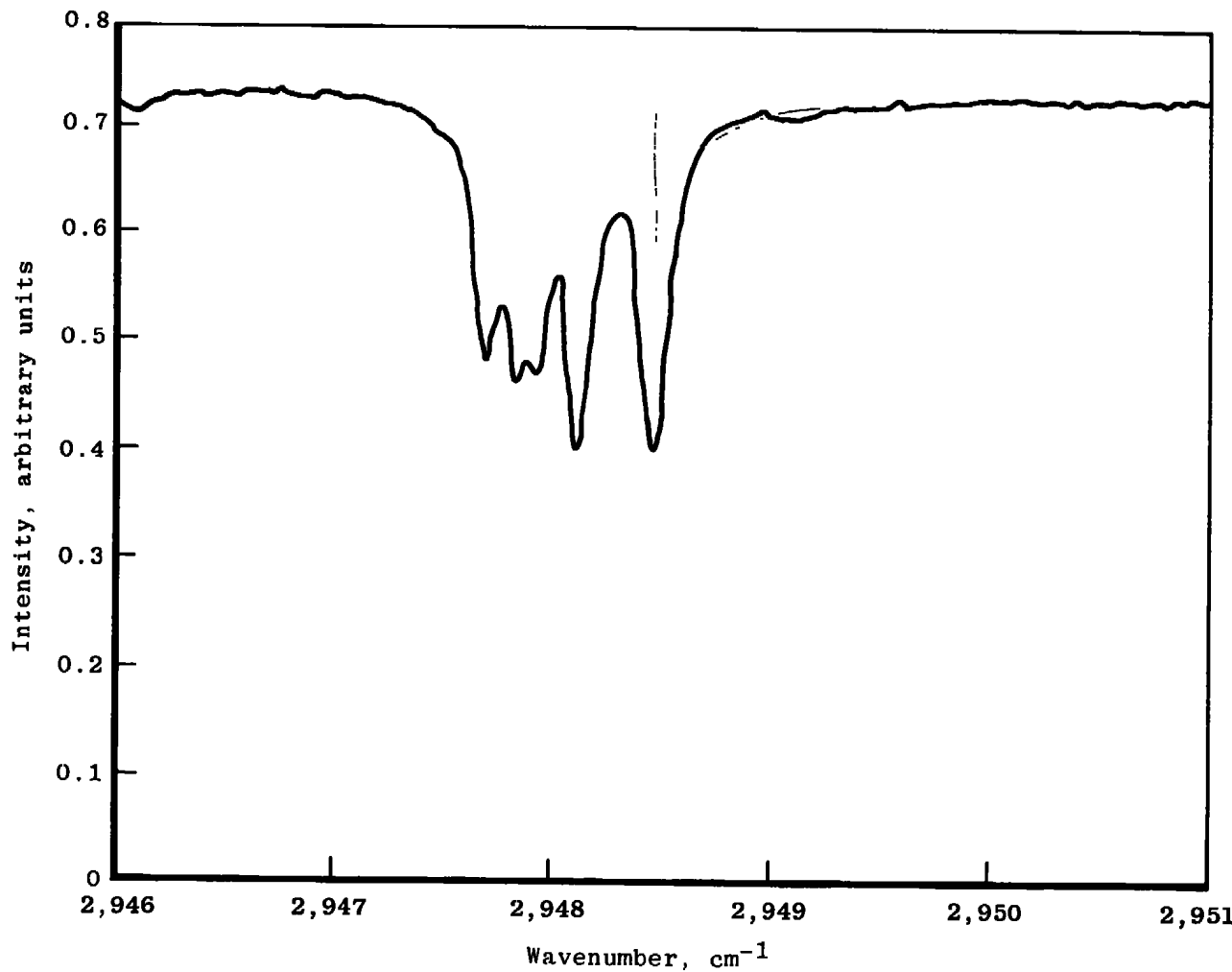
Figure 19. Absorption spectrum of methane in nitrogen at 297°K, P₅ line, methane concentration 996 ppm, pressure 97.9 kPa, pathlength 50.7 cm.

InSb Detector
System

Filter

Beam
Chopper

Transmission
Detector

3.39-μ He-Ne Laser

Reference
Detector

Beam
Splitter

Filter
Radiometer

White
Multiple-
Pass
System

Portable
Absorption
Cell
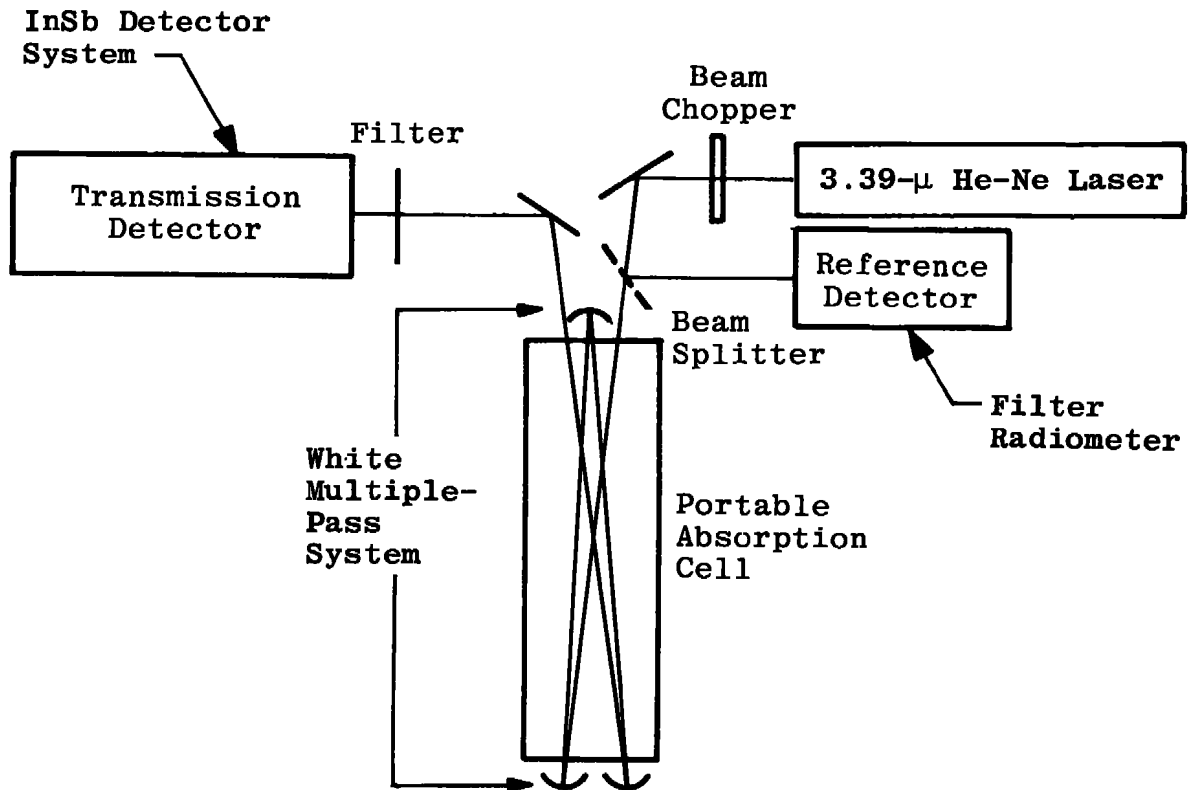
Figure 20. Schematic diagram of IR laser experiment.
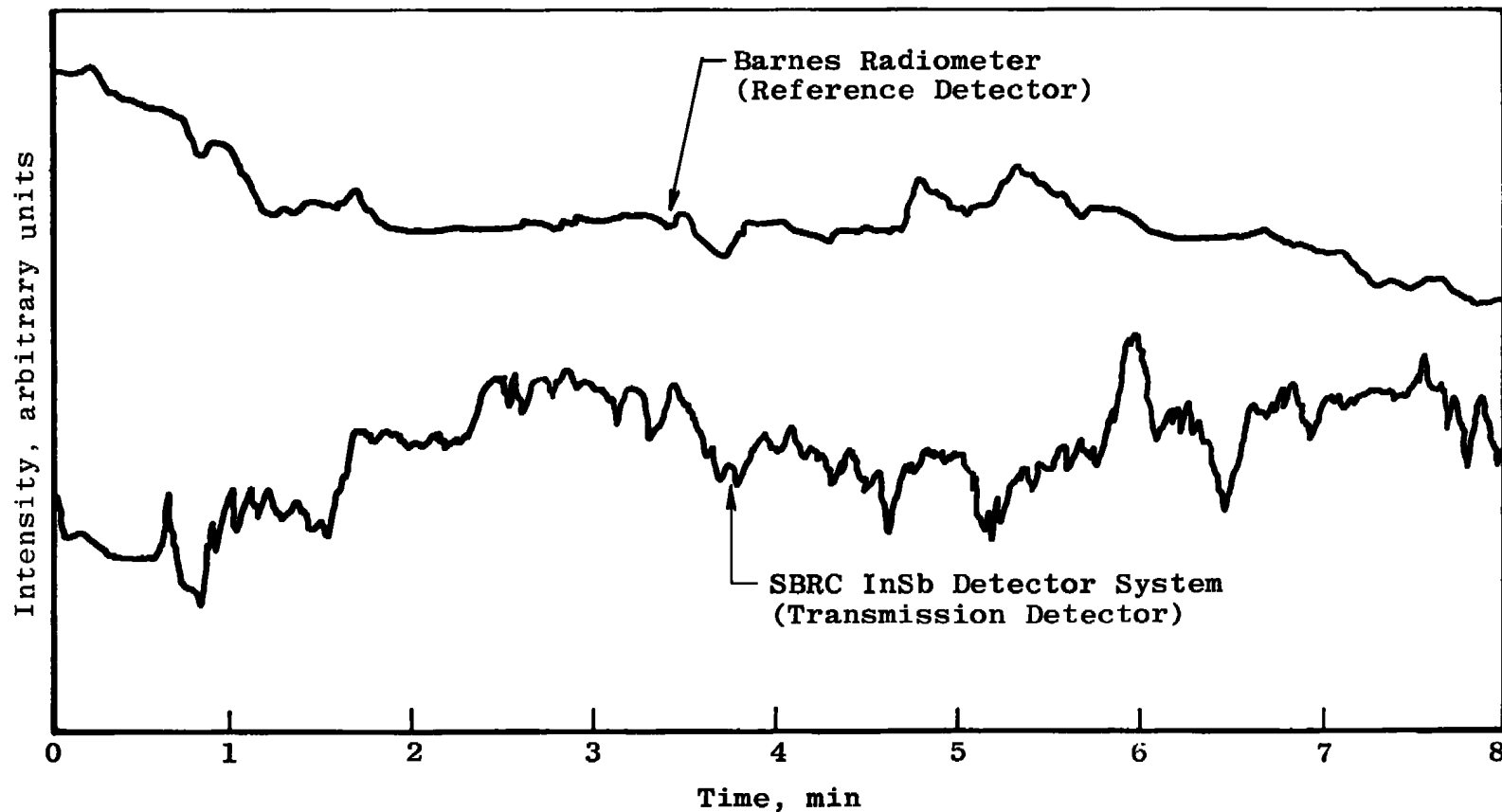
Figure 21. Simultaneous recordings of He-Ne IR laser power monitors; upper trace, filter radiometer; lower trace, InSb detector system, chart speed 2.54 cm·min⁻¹.

Strip
Chart
Recorder

Dove (Inverting)
Prism

Entrance Slit

Mirror

Spectrometer
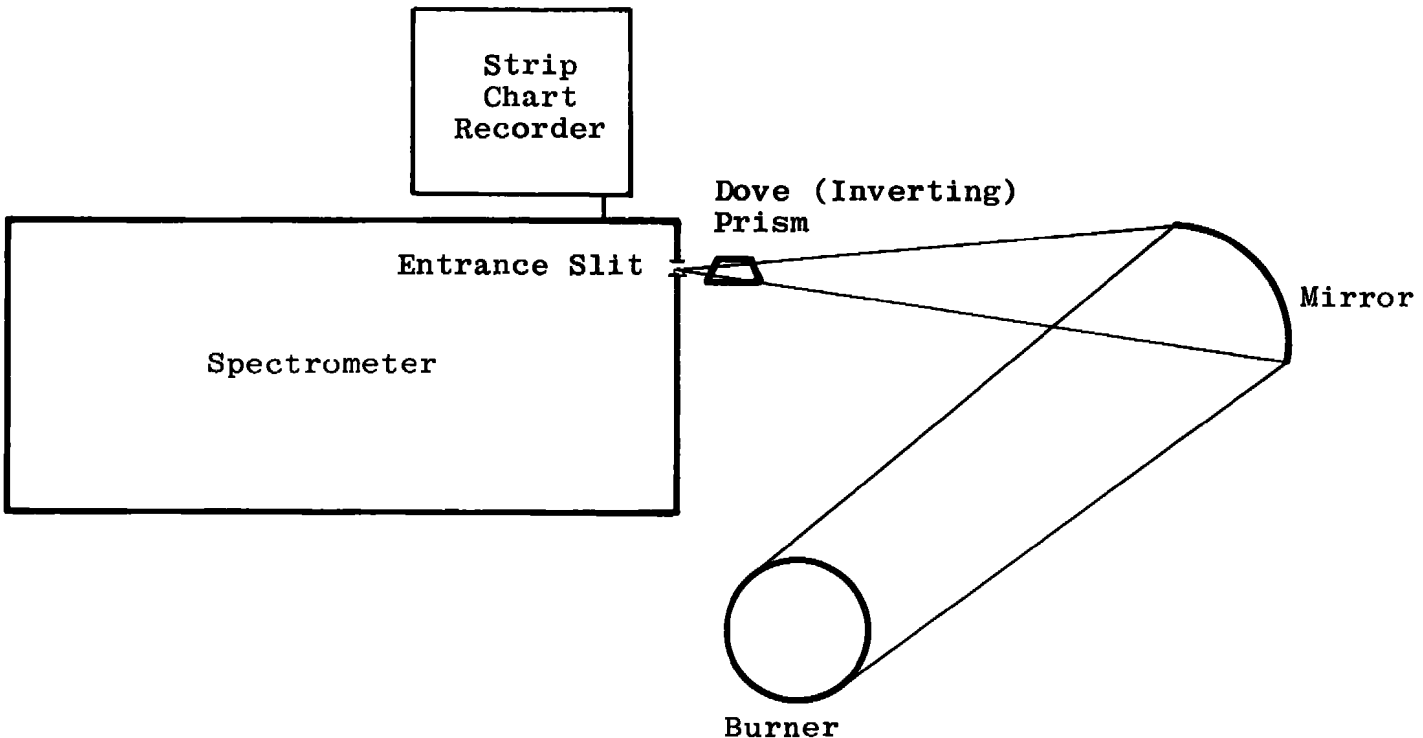
Burner

Figure 22. Schematic of CH emission experiment.
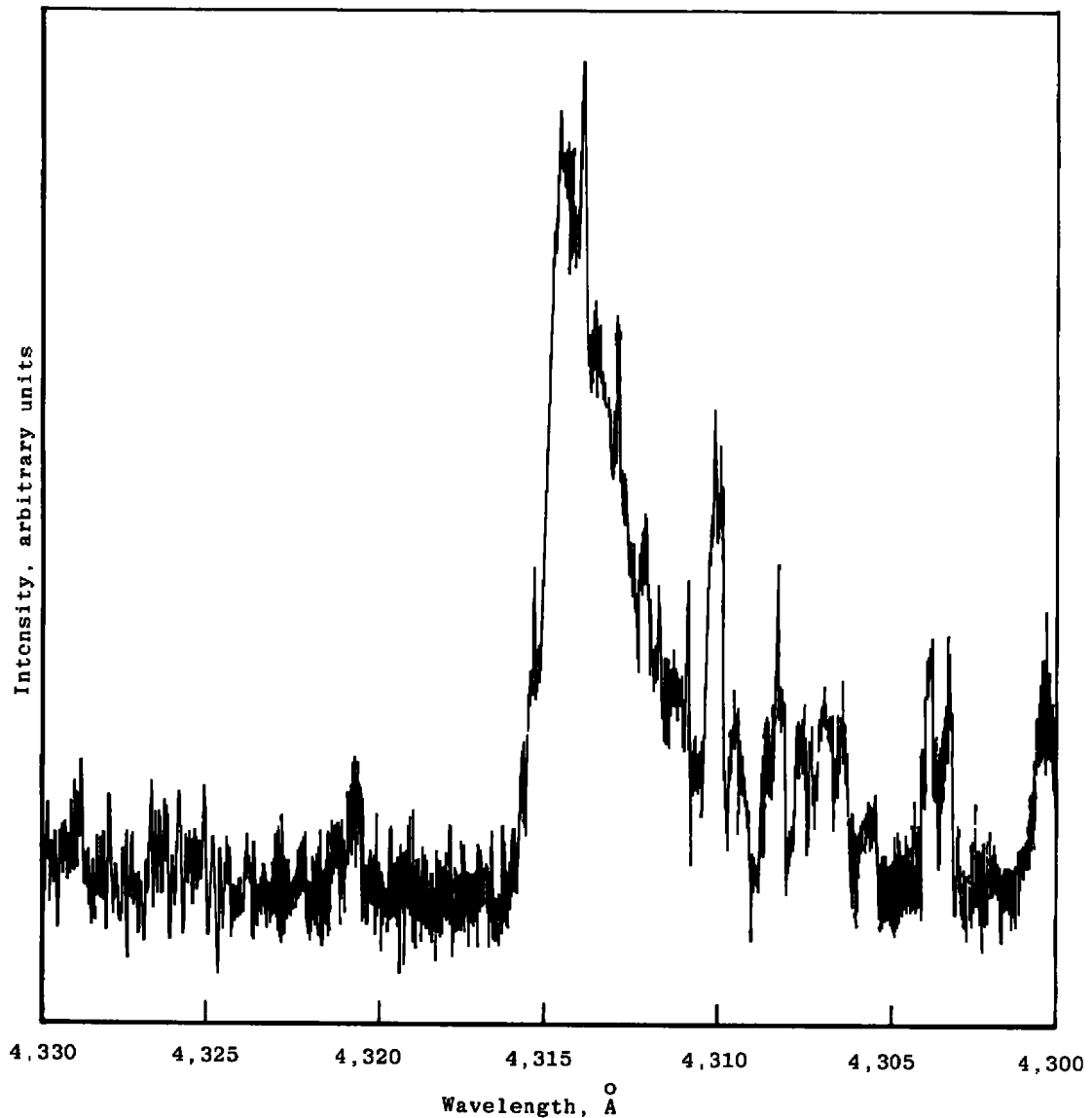
Figure 23. CH emission spectrum at burner surface, methane
stoichiometric flame, scale 1 cm = 2.94Å.
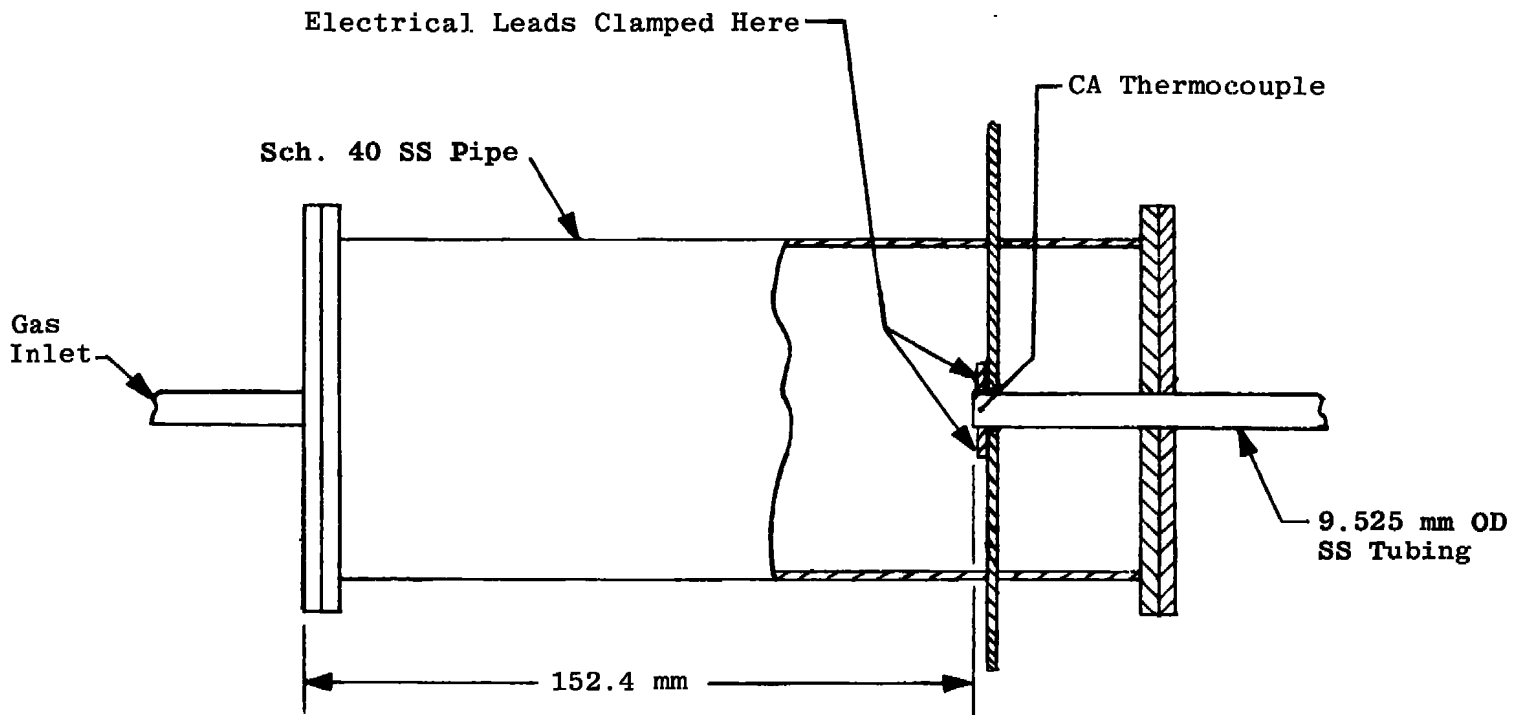
Figure 24. Probe simulator.
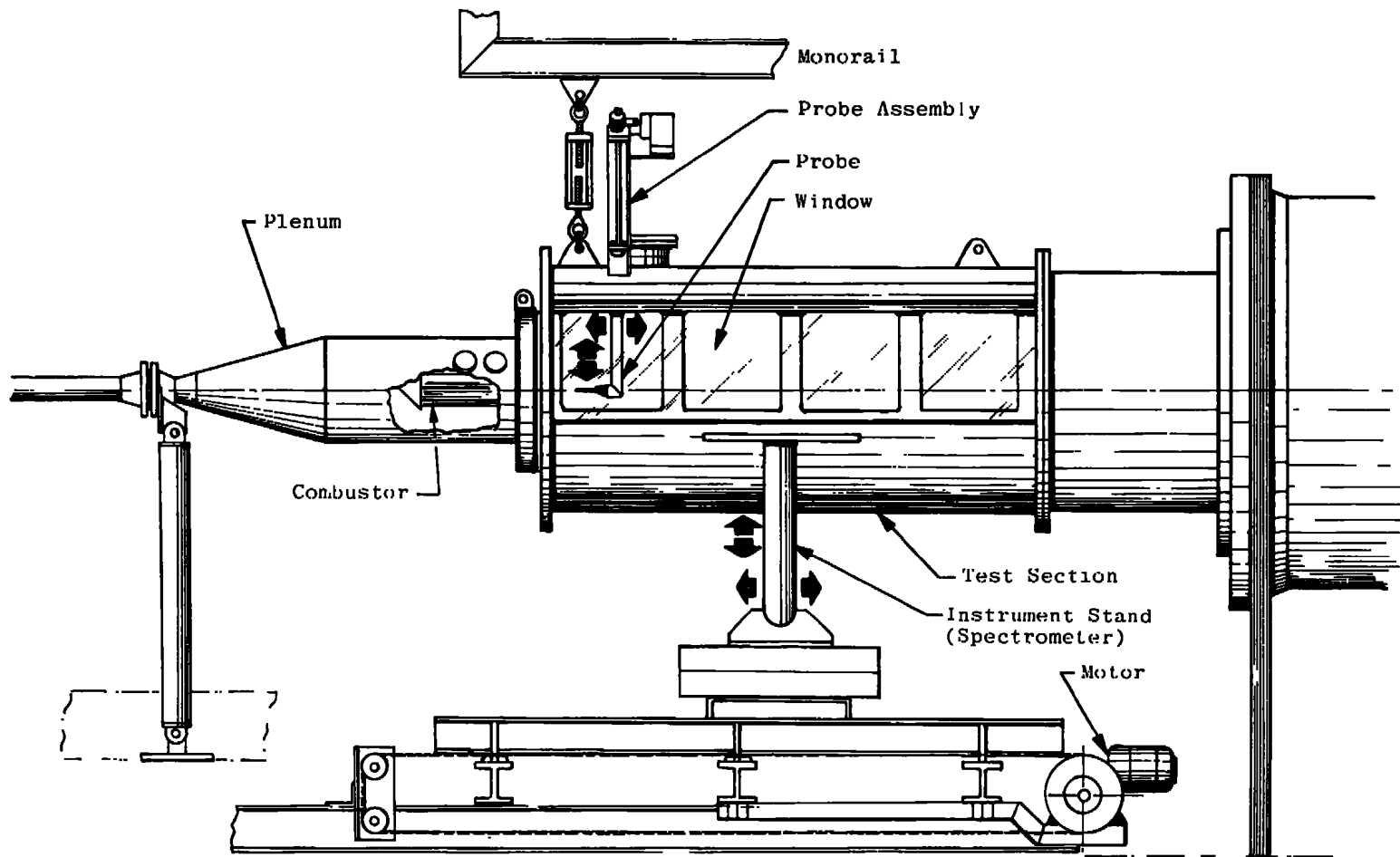
Figure 25. Diagram of R-2C-1 Research Cell.
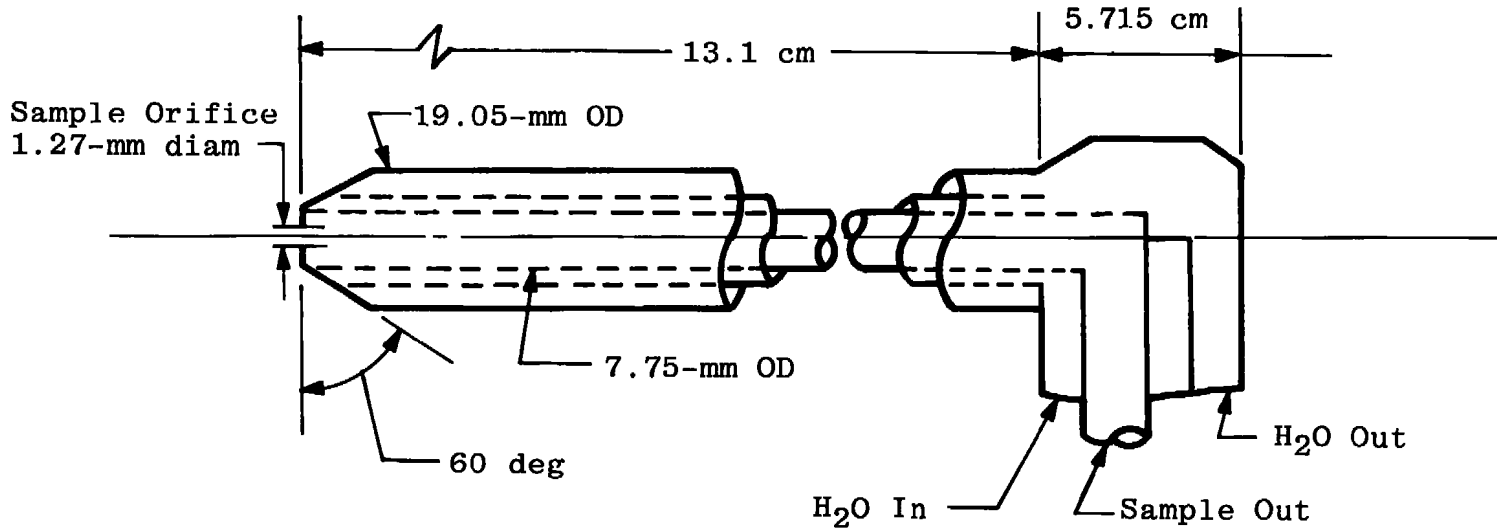
Figure 26. Diagram of emissions probe.

Table 1. Methane Thermal Depopulation Factors (Relative to 300° K)

Temperature, $^{\circ}$K	Line	Rotational Factor	Vibrational Factor	Total Thermal Depopulation Factor
300	R_6	1	1	1
300	R_7	1	1	1
573	R_6	0.627	0.857	0.537
573	R_7	0.741	0.857	0.635
773	R_6	0.462	0.667	0.308
773	R_7	0.573	0.667	0.382
1,000	R_6	0.345	0.458	0.158
1,000	R_7	0.441	0.458	0.202
1,500	R_6	0.209	0.172	0.0164
1,500	R_7	0.276	0.172	0.0474
2,000	R_6	0.143	0.0617	0.00883
2,000	R_7	0.193	0.0617	0.0119

Table 2. Methane Detectability Limits (PPM) at One Atmosphere

Temperature, ^{o}K, and Line		Pathlength, m		
		1	10	50
300	R_6	5.80	0.580	0.116
	R_7	7.24	0.724	0.145
573	R_6	20.8	2.08	0.416
	R_7	21.8	2.18	0.436
773	R_6	48.9	4.89	0.978
	R_7	48.9	4.89	0.978
1,000	R_6	153	15.3	3.06
	R_7	112	11.2	2.24
1,500	R_6	822	82.2	16.4
	R_7	764	76.4	15.3
2,000	R_6	4,419	442	88.4
	R_7	4,065	406	81.3

Table 3. Estimated THC Detectability Limits (PPM) at One Atmosphere

Temperature, °K	Pathlength, m		
	1	10	50
300	387	38.7	7.73
573	1,387	139	27.7
773	3,260	326	65.2
1,000	7,470	747	149
1,500	50,900	5,090	1,020
2,000	271,000	27,100	5,420

Table 4. R-2C-1 Combustor Exhaust Results

Position Downstream of Nozzle, cm	THC On-Line Analysis (FID), ppm	THC Lab Analysis (FID), ppm	Methane Lab Analysis (Gas Chromatograph)
33.6	6.9	3.5	None detected
66.0	7.1	3.6	None detected
127.0	11.5	3.5	None detected

APPENDIX A
CURVE OF GROWTH CALCULATION PROBLEM

```
C    CURVE OF GROWTH CALCULATION PROGRAM
C    ****************************************************************
C
C      THIS PROGRAM CALCULATES THE CURVE OF GROWTH FOR USER SUPPLIED
C      BROADENING PARAMETERS, A.  THE A VALUES ARE ENTERED ONE PER CARD IN A
C      D12.5 FORMAT.
C
C      THE INTEGRATION OF THE ABSORBANCE IS TERMINATED WHEN THE VALUE OF THE
C      ABSORBANCE IS 1D-5 OR LESS OF THE CENTER VALUE OR WHEN 10,000 CM-1
C      IS REACHED.
C
C      THE OUTPUT IS-
C
C      FIRST COLUMN- LOG OF REDUCED DENSITY FUNCTION (LOGX)
C      SECOND COLUMN- REDUCED DENSITY FUNCTION (X)
C      THIRD COLUMN- LOG OF REDUCED INTEGRATED ABSORBANCE (LOGY)
C      FOURTH COLUMN- REDUCED INTEGRATED ABSORBANCE (Y)
C      FIFTH COLUMN- END OF INTEGRATION LIMIT REACHED? 1-YES,   2-NO
C      SIXTH COLUMN- INTEGRATION LIMIT
C
C      FOR DEFINITION OF ABOVE VARIABLES AND DEVELOPMENT OF THE FORMULI
C      USED SEE-
C      'RESONANCE RADIATION AND EXCITED ATOMS' BY A.C.G. MITCHELL AND
C      M.W. ZEMANSKY,  PAGES 130 TO 133   (1934, MACMILLAN)
C
C      INTEGRATION SUBROUTINES ARE RENAMED IBM SCIENTIFIC SUBROUTINE
C      GAUSSIAN QUADRATURE (DQG32) SUBROUTINES.
C
       IMPLICIT REAL *8(A-H,O-Z)
       COMMON A,W,XKO
       EXTERNAL  XABS
     1 READ(5,10,END=9999) A
       PRINT 20
       PRINT 30, A
       PRINT 50
       XLP=0.0D0
       XP=1.0D0
       DO 2 IA =1,25
       XNF= 1.1312463D09 *XP
       XKO=8.315645D-12*XNF
       XO=XABS(0.0D0)
       AR=0.0D0
       DO 5 I=1,2000
       AR =AR+5.0D0
       XK=XABS(AR)/XO
       IF(XK.LT.1.0D-5) GO TO 6
     5 CONTINUE
       XLT=-10000.0D0
       XUT=10000.0D0
       IND=1
       GO TO 7
     6 XLT=-1.0D0*AR
       XUT=AR
       IND=0
```

```
   7 CONTINUE
     XABST=0.0D0
     XR=(XUT -XLT)/20.0D0
     XL=XLT-XR
     DO 8 I= 1,20
     XL=XL+XR
     XU=XL +XR
     CALL ADQG32(XL,XU,XABS,XABSI)
     XABST=XABST+XABSI
   8 CONTINUE
     XABSI = XABST
     XFAG=XABSI* 1.3250518D0
     XLFAG= DLOG10(XFAG)
     PRINT 60, XLP,XP,XLFAG,XFAG,IND,XU
     XLP=XLP + .25D0
     XP= 10.0D0**XLP
   2 CONTINUE
     GO TO 1
  10 FORMAT(D12.5)
  20 FORMAT(1H1 )
  30 FORMAT(' CURVE OF GROWTH CALCULATION FOR A= ',D12.5,//)
  50 FORMAT('         LOGX              X              LOGY            Y',/)
  60 FORMAT(1X,4(2X,D15.6),2X,I1,2X,D10.2)
9999 STOP
     END




     FUNCTION XABS(X)
     IMPLICIT REAL * 8(A-H,O-Z)
     COMMON A,W,XK0
     W=2.0D0*X*8.325546D0
     XA=A
     XW=W
     CALL VOIGT(XA,XW,ZINT)
     XKV=XK0*ZINT
     XABS=(2.0D0*3.1415927D0)*(1.0D0 -DEXP(-10.0D0*XKV))
     RETURN
     END
```

60

```
SUBROUTINE VOIGT(XA,XW,ZINT)
IMPLICIT REAL * 8 (A-H,O-Z)
COMMON A,W,XKO
EXTERNAL H
XL=-6.0D0
XU=6.0D0
XS=0.0D0
CALL BDQG32(XL,XS,H,Y)
Z=Y
CALL BDQG32(XS,XU,H,Y)
ZINT = Z + Y
RETURN
END
```

```
FUNCTION H(X)
IMPLICIT REAL * 8 (A-H,O-Z)
COMMON A,W,XKO
H=((A/3.1415927D0)*DEXP(-1.0D0*(X**2)))/(A**2 +((W-X)**2))
RETURN
END
```

```
      SUBROUTINE ADQG32(XL,XU,FCT,Y)
C                                                                     DG32 370
C                                                                     DG32 380
      DOUBLE PRECISION XL,XU,Y,A,B,C,FCT                              DG32 390
C                                                                     DG32 400
      A=.5D0*(XU+XL)                                                  DG32 410
      B=XU-XL                                                         DG32 420
      C=.49863193092474078D0*B                                       DG32 430
      Y=.35093050047350483D-2*(FCT(A+C)+FCT(A-C))                    DG32 440
      C=.49280575577263417D0*B                                       DG32 450
      Y=Y+.81371973654528350-2*(FCT(A+C)+FCT(A-C))                   DG32 460
      C=.48238112779375322D0*B                                       DG32 470
      Y=Y+.1269603265463103OD-1*(FCT(A+C)+FCT(A-C))                  DG32 480
      C=.46745303796886984D0*B                                       DG32 490
      Y=Y+.17136931456510717D-1*(FCT(A+C)+FCT(A-C))                  DG32 500
      C=.44816057788302606D0*B                                       DG32 510
      Y=Y+.21417949011113340D-1*(FCT(A+C)+FCT(A-C))                  DG32 520
      C=.42468380686628499D0*B                                       DG32 530
      Y=Y+.25499029631188088D-1*(FCT(A+C)+FCT(A-C))                  DG32 540
      C=.39724189798397120D0*B                                       DG32 550
      Y=Y+.29342046739267774D-1*(FCT(A+C)+FCT(A-C))                  DG32 560
      C=.36609105937014484D0*B                                       DG32 570
      Y=Y+.32911111388180923D-1*(FCT(A+C)+FCT(A-C))                  DG32 580
      C=.33152213346510760D0*B                                       DG32 590
      Y=Y+.36172897054424253D-1*(FCT(A+C)+FCT(A-C))                  DG32 600
      C=.29385878862038116D0*B                                       DG32 610
      Y=Y+.39096947893535153D-1*(FCT(A+C)+FCT(A-C))                  DG32 620
      C=.25344995446611470D0*B                                       DG32 630
      Y=Y+.41655962113473378D-1*(FCT(A+C)+FCT(A-C))                  DG32 640
      C=.21067563806531767D0*B                                       DG32 650
      Y=Y+.43826046502201906D-1*(FCT(A+C)+FCT(A-C))                  DG32 660
      C=.16593430114106382D0*B                                       DG32 670
      Y=Y+.45586939347881942D-1*(FCT(A+C)+FCT(A-C))                  DG32 680
      C=.11964368112606854D0*B                                       DG32 690
      Y=Y+.46922199540402283D-1*(FCT(A+C)+FCT(A-C))                  DG32 700
      C=.72235980791398250-1*B                                       DG32 710
      Y=Y+.47819360039637430D-1*(FCT(A+C)+FCT(A-C))                  DG32 720
      C=.24153832843869158D-1*B                                       DG32 730
      Y=B*(Y+.48270044257363900D-1*(FCT(A+C)+FCT(A-C)))              DG32 740
      RETURN                                                         DG32 750
      END                                                            DG32 760
```

```
      SUBROUTINE BDQG32(XL,XU,FCT,Y)                                      DG32 370
C                                                                        DG32 380
C                                                                        DG32 390
      DOUBLE PRECISION XL,XU,Y,A,B,C,FCT                                 DG32 400
C                                                                        DG32 400
      A=.5D0*(XU+XL)                                                     DG32 410
      B=XU-XL                                                            DG32 420
      C=.49863193092474078D0*B                                          DG32 430
      Y=.35093050047350483D-2*(FCT(A+C)+FCT(A-C))                       DG32 440
      C=.49280575577263417D0*B                                          DG32 450
      Y=Y+.81371973654528350-2*(FCT(A+C)+FCT(A-C))                      DG32 460
      C=.48238112779375322D0*B                                          DG32 470
      Y=Y+.12696032654631030D-1*(FCT(A+C)+FCT(A-C))                     DG32 480
      C=.46745303796886984D0*B                                          DG32 490
      Y=Y+.17136931456510717D-1*(FCT(A+C)+FCT(A-C))                     DG32 500
      C=.44816057788302606D0*B                                          DG32 510
      Y=Y+.21417949011113340D-1*(FCT(A+C)+FCT(A-C))                     DG32 520
      C=.42468380686628499D0*B                                          DG32 530
      Y=Y+.25499029631188088D-1*(FCT(A+C)+FCT(A-C))                     DG32 540
      C=.39724189798397120D0*B                                          DG32 550
      Y=Y+.29342046739267774D-1*(FCT(A+C)+FCT(A-C))                     DG32 560
      C=.36609105937014484D0*B                                          DG32 570
      Y=Y+.32911111388180923D-1*(FCT(A+C)+FCT(A-C))                     DG32 580
      C=.33152213346510760D0*B                                          DG32 590
      Y=Y+.36172897054242530D-1*(FCT(A+C)+FCT(A-C))                     DG32 600
      C=.29385787862038116D0*B                                          DG32 610
      Y=Y+.39096947893535153D-1*(FCT(A+C)+FCT(A-C))                     DG32 620
      C=.25344995446611470D0*B                                          DG32 630
      Y=Y+.41655962113473378D-1*(FCT(A+C)+FCT(A-C))                     DG32 640
      C=.21067563806531767D0*B                                          DG32 650
      Y=Y+.43826046502201906D-1*(FCT(A+C)+FCT(A-C))                     DG32 660
      C=.16593430114106382D0*B                                          DG32 670
      Y=Y+.45586939347881942D-1*(FCT(A+C)+FCT(A-C))                     DG32 680
      C=.11964368112606854D0*B                                          DG32 690
      Y=Y+.46922199540402283D-1*(FCT(A+C)+FCT(A-C))                     DG32 700
      C=.72235980791398250-1*B                                          DG32 710
      Y=Y+.47819360039637430D-1*(FCT(A+C)+FCT(A-C))                     DG32 720
      C=.24153832438691580-1*B                                          DG32 730
      Y=B*(Y+.48270044257363900D-1*(FCT(A+C)+FCT(A-C)))                 DG32 740
      RETURN                                                            DG32 750
      END                                                               DG32 760
```

NOMENCLATURE

a	Broadening parameter
$A_G/2\pi$	Integrated absorbance, cm^{-1}
c	Speed of light, cm/sec
c_i	Number of carbon atoms of species i
e	Electron charge, esu
f_{300}	Population-corrected f-number
f_i	F-number (line strength parameter) of transition i
g_i	Vibrational degeneracy of state i
J	Rotational quantum number
ℓ	Pathlength, cm
M	Molecular weight, amu
m	Electron mass, gm
N_D	Number density of diluent gas, molecules/cm^3
N_i	Number density of absorbing molecules in state i, molecules/cm^3
N_s	Standard number density, molecules/cm^3
P_a	Pascal, unit of measure for pressure; 101.325 kPa = 1 atm = 14.7 psia
P_D	Pressure of diluent gas, kPa
$p_i(T)$	Fractional population of state i at temperature T
P_n	n^{th} spectral line of the P branch
Q_{vT}	Vibrational partition function at temperature T
R	Universal gas constant
R_n	n^{th} spectral line of the R branch

S_J Line strength, $cm^{-2}-atm^{-1}$

T Static temperature, °K

a Molecular absorption coefficient, $cm^2 molecule^{-1}$

$\Delta\nu_c$ Collisional width of spectral line, cm^{-1}

$\Delta\nu_D$ Doppler width of spectral line, cm^{-1}

ν_i Vibrational frequency of state i, cm^{-1}

ν_o Absorption line center frequency, cm^{-1}

ϕ Equivalence ratio